# Chapter 1

# Introduction

## 1.1 Liquid crystal display

Thin-film transistor liquid crystal display (TFT-LCD) is widely used for mobile phones, personal computers, personal digital assistants (PDAs), note book, and TVs. On the size, the LCD is developed with the features of light weight, thin format, and compact size. In character, the LCD has low consumption, high definition, and easy to develop large size and portable display. Several LCD modes have been developed such as: Twist nematic (TN), multi-domain vertical alignment (MVA) [1-3], in-plane switching (IPS) [4-5], Nonchiral-smetic-C (NSC) [6], optically compensated bend (OCB) [7], ferroelectric liquid crystal (FLC) displays [8]. Among these modes, the TN is first adopted for display application for its low driving voltage and gray scales capability.

For the TN mode as shown in Fig 1.1, the alignment directions of the liquid crystal molecules are twisted through 90° on alignment layers on both transparent electrodes. In the absence of an electric field, the nematic director undergoes a 90 degree twist within the cell. Unpolarized light enters the first polarizing filter and emerges polarized in the same direction as the local orientation of the liquid crystals molecules. The twisted structure of the liquid crystals molecules within the cell then acts as an optical wave guide and rotates the plane of polarization by a quarter turn so that the light which reaches the analyzer can pass through it. This state is called bright state. When an electric filed is applied to the cell, the liquid crystal molecules tend to align with the resulting electric field E and the optical wave guiding property of the cell is lost. Thereby the light can not pass through the analyzer that this is called dark state.

By adopting this structure, displays offering high contrast and low driving voltage can be realized. But when it applies TV, the image quality is limited with the slow response time and viewing angle. Based on these questions, ferroelectric liquid crystal display was considered as promising solution because the FLC is demonstrated with special properties of sub-micro second response, wide viewing angle, bi-stable. In particular, the fast response can reduce the motion blur from moving picture, and to suppress color break-up phenomenon in filed sequential color (FSC) LCD [9]. However, the issues such as driving voltage, working temperature, free defect, and assembly processes are impeded the applications of FLCD. Therefore, to realize FLC in display application remains great challenges.

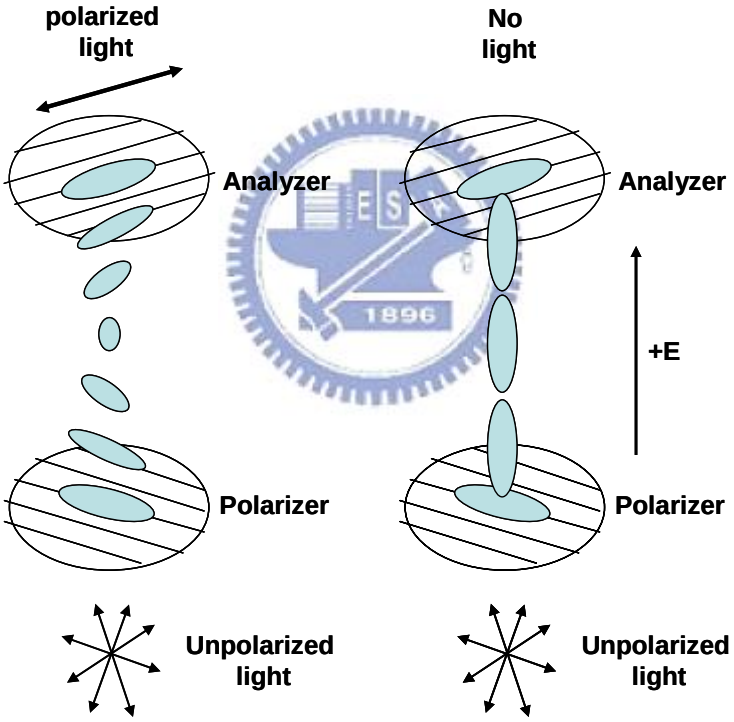


Fig. 1.1. The TN device geometry and operation.

## 1.2 Liquid crystal phase

The discovery of the liquid crystal can be retraced by 1888, Austrian plant scholar F Reinitzer at that time used sour in the storax that heated the cholesterol and found the unusual phenomenon of melting by accident. Thereafter German physicist O. Lehmann used heated polarizing optical microscope to observe this muddy state, found this substance with optic anisotropic and verified it is one of crystalline liquid. Namely this muddy state has a structure that is similar to molecule of crystal and also has liquid flowing characteristic. Later the existence of the liquid crystal is demonstrated and has begun the research of the liquid crystal. Liquid crystal is namely liquid crystallization, its behavior is among liquid (same direction) and solid (crystallization), and its state is called mesophase. The molecule of this state arranges certain movement regulation. That is to say, dynamic crystal has unstable optics character and is very easy to influence by external field for instance electric field, magnetic field, temperature, pressure then further produce optics effect.

Two main types of liquid crystal are Thermotropic liquid crystals and Lyotropic liquid crystals. Thermotropic liquid crystals are provided with stable phase at certain temperature range. So it can control liquid crystal temperature to make phase change. In the same way, Lyotropic liquid crystals mix certain the solvent (usually uses water for solvent) according to difference of concentration and have certain stable phase.

Most experiments are to take Thermotropic liquid crystals as the core. Under the different temperature ranges, the liquid crystal molecular has different phase structure. In 1922, G.. Friedel used the results observed polarizing optical microscope, depended on it under different temperature ranges and divided the arrangement structure of the liquid crystal molecule into three kinds - Smectic, Nematic, Cholesteric. It explains to classify on its structure below as:

(a) Smectic Phase

As shown in Fig 1.2 (a), the rod-shaped molecule forms layer structure, every layer of molecule long axis directions is approximately parallel, and perpendicular to the plane or has an angle of inclination on the plane. The molecule long axis direction is perpendicular to the plane is called Smectic-A, and having an angle of inclination on the plane is called Smectic-C. Its order parameter is close to 1 convergence. Action of layer with each other in Smectic liquid crystal can be destroyed because of temperature increased; layer with each other is easier to slip. Action of molecule in every layer is so strong that it is not to be easily interrupted. From a single layer, it not only arranges in order but also has greater viscosity.

(b)Nematic phase

As shown in Fig 1.2 (b), the rod-shaped molecule is approximately parallel arrangement with certain direction and doesn't have layer structure. Its arrangement is non-order than Smectic liquid crystal. In the same way, its order parameter is smaller than Smectic. As viscosity is smaller, it can easily flow.

(c)Cholesteric

As shown in Fig 1.2 (c), this phase is discovered in the cholesteric that arrangement of inter molecule is similar to nematic phase and possess twist structure. If molecule rotates one round (360 degrees) distance is called pitch.

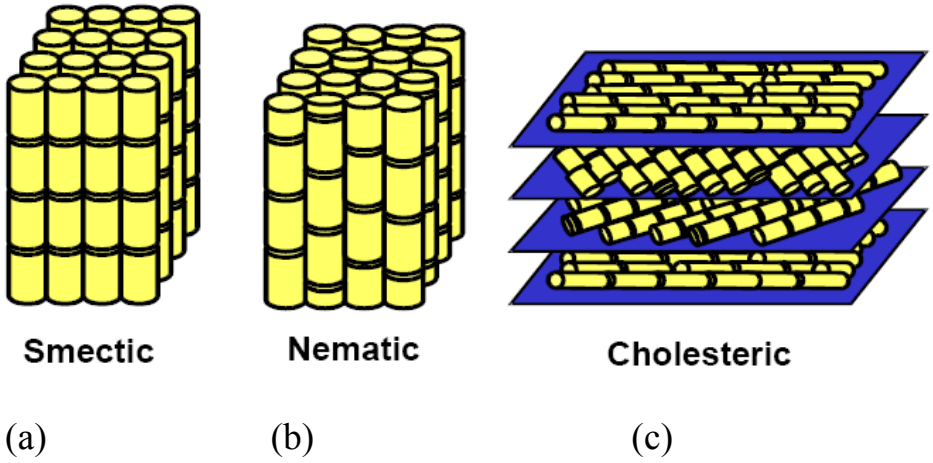


**Fig.1.2.** Molecular arrangement structure of liquid crystal phases.

## 1.3 Ferroelectric liquid crystal

In the SmC* phase, which is a SmC phase consisting of chiral molecules, but not racemic. The helix is formed by a precession of the tilt about an axis normal to the layers, as shown Fig1.3. The tilt direction of the molecules in a layer above or below an object layer is rotated through an azimuthal (Ψ) relative th the object layer. This rotation always occurs in the same direction for a particular material, thus forming a helix. The helix can be either right-handed or left-handed depending on the chirality of the constituent molecules.

The periodicity of the the helix, called the pitch, often increases somewhat with increasing temperature, but the variation might be much more complex and varies from compound to compound. The pitch length of the helix form most SmC* phases is commonly greater than one micrometer, indicating that a full twist of the helix s made up of many thousands of layers. Thus, the azimuthal angle (Ψ) is relatively small and is usually on the order of one-tenth to one-hundredth of a degree.

FLC also exhibits a net spontaneous polarization which is originated in the $C_2$ symmetry of the SmC* phase perpendicular to both the molecular director and the layer normal, so that over macroscopic distances (few microns) the polarization averages to zero. Since the coupling of the polarization to applied fields is linear in the field, this means that FLC can be made to switch quickly and in a bipolar manner. This makes FLC ideally suited to electro-opic applications. FLC are now included in several display technologies, the most popular of which use the surface-stabilized (SSFLC) [10] geometry.

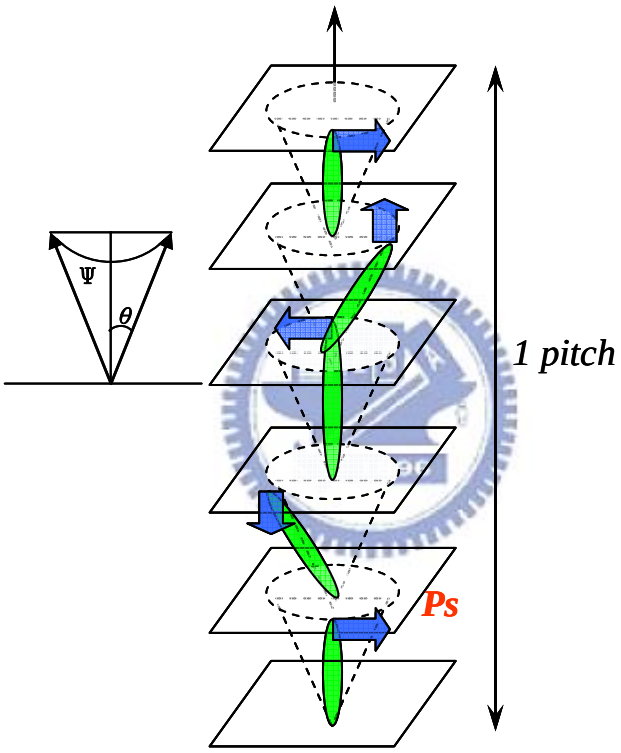


Fig. 1.3. The structure of the chiral smectic C* phase.

## 1.4 Motivation and Objective

The FLC of its advantages of fast switching, wide viewing angle and bistable capability is suitable for field sequential color LCD (FSC-LCD). The fast switching of characteristic of FLC can be applied effectively to reduce the motion blur and to suppress color break-up phenomenon. However, the issue such as operating voltage, defect free structures, temperature and assembly processes are hindered the applications of FLCD. For that reason, the main objective of this thesis is to understand the molecule orientation state and the causes of zigzag and horizontal defect. Then study of eliminating defects would obtain mono-domain in SSFLC devices.

## 1.5 Organization of this Thesis

This thesis is organized as following: the molecular orientation related orientation structure, chevron structure and defects in SSFLC, a study of mono-domain to eliminate these defects are introduced in Chapter 2. The experimental process and the introduction of measurement instruments and their principles will be given in Chapter 3. The discussions of the experimental results are also presented in the Chapter 4. Finally, the conclusion is summarized in Chapter 5.

# Chapter 2

# Surface Stabilized Ferroelectric Liquid Crystal (SSFLC)

## 2.1 Introduction

The surface stabilized ferroelectric liquid crystal (SSFLC) was proposed to suppress the helix by Clark and Lagerwall in 1980 [10]. The SSFLC is sandwiched between two substrates separated by around 2 $\mu$m, in which the helical structure of the FLC material is unwound. The helix is constrained by cell gap that is less than the helical pitch because the interaction forces between the liquid crystal and the bounding plates unwind the intrinsic helix.

The switching of SSFLC is achieved by applying an electric field that induces changes in the director orientation. Since the polarization vector is coupled to the director, it is also switched between the two stable states by the electric field as shown Fig 2.1. The down state with the director parallel to the polarizer is non transmissive while the other allows light to cross the cell. In the up state, light is transmitted because the director is no longer parallel to the polarizer and one component of the polarization has been retarded by 180 degrees, therefore the light passes thorough the analyzer on the top. The intensity of light is dependent on the cone angle, delta n, cell thickness, and wavelength of the light as below formula.

$$I = I_o \sin^2 4\theta \sin^2 (\pi \Delta n T / \lambda)$$

where

$I_o$ is the initial intensity

$\theta$ is the cone angle

$\Delta n$ is the birefringence

T is the cell thickness

$\lambda$ is the wavelength.

In the application, SSFLC possess excellent properties, such as fast switching speed and wide viewing angle. These properties are indispensable for high-quality displays. Beside the memory property and large hysteresis are inadequate for active matrix driving, and the alignment mechanism of SSFLC is very difficult and complicated. In following section, it will describe and realize the orientation structure, chevron structure, zigzag defect and horizontal defect first. Then we discuss how to eliminate defects and get better alignment base on many groups have investigated and proposed methods.

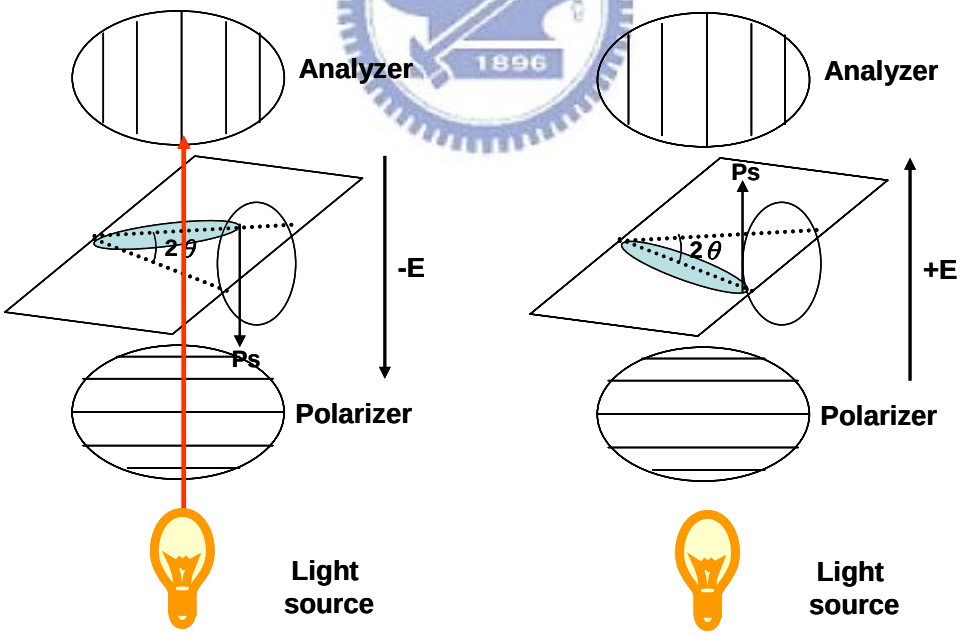


Fig. 2.1. The construction and operation of the SSFLC cell.

## 2.2 Molecular Orientation States

### 2.2.1 Orientation structures

The orientation structures of ferroelectric liquid crystal have uniform, helical and splay (or call twist) state [11], as shown in Fig 2.2. Uniform state exhibits that the molecule director is parallel to the substrate in every layer, but it possibly has two different parallel direction with the cone angle $0^{\circ}$ and $180^{\circ}$. In other words, the direction of spontaneous polarization, up or down direction is perpendicular to the surface. Helical state shows that the molecule director spirals in z axis direction, the position of molecule director is changed by different z axis direction. In splay state, the molecule director twist in x axis direction, the molecule director varies position following the different x axis direction. The uniform and helical state is often in the very thin cell, and splay state exists in rather thicker cell.

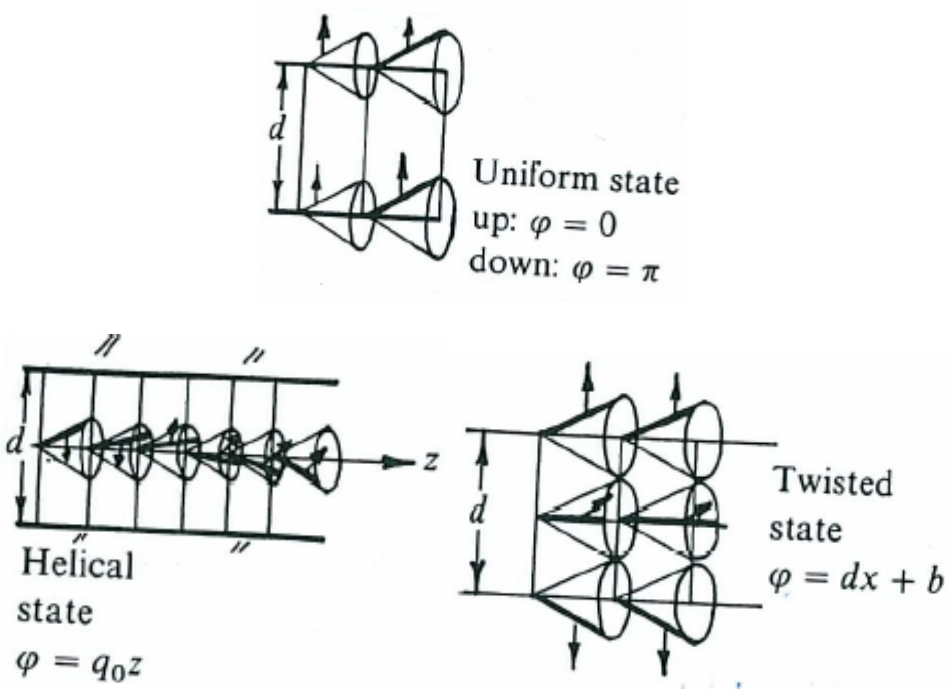


Fig. 2.2. Phase diagram of FLC states [11].

### 2.2.2 Chevron Structures

Layer structure strongly depends on the surface alignment as shown in Fig.2.3 [12]. In a homeotropic aligning cell, the smectic layer is parallel to the substrates and schlieren texture is observed by polarizing optical microscope. In planar homogeneous cell, the oblique layer structure is formed by antiparallel aligning cell. Chevron shape layer structure is formed by using Parallel alignment in most SSFLCs configuration [13], which was found by Rieker *et al.* using X-ray measurements [14].

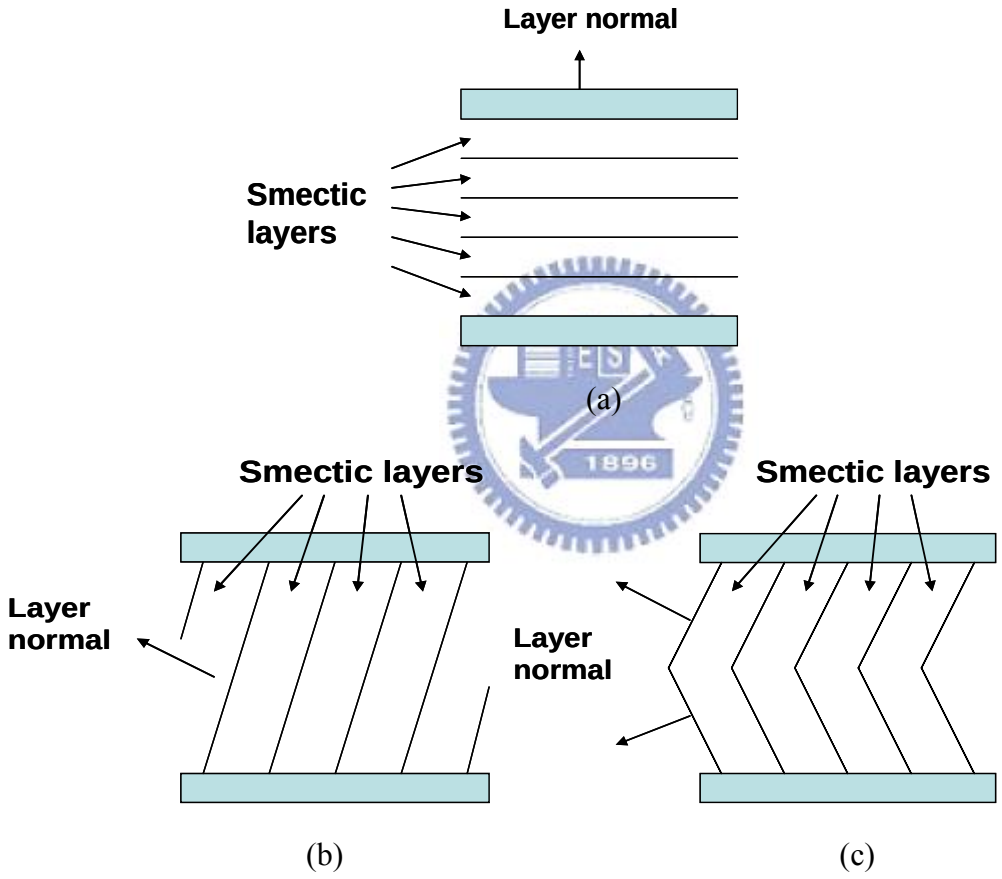


**Fig.2.3.** Cross section of smectic layer structures in various alignment cells. (a) Homeotropic (b) Oblique (c) Chevron.

The origin of chevron layer structure is explained by discrepancy between the layer spacing of the SmC* phase and that of the high temperature SmA phase [15-16]. The SmA phase usually forms in the uniform book-shelf geometry, where the layers are normal to the

substrates and the molecular director is oriented parallel to the substrates. Upon cooling to the SmC* phase, the spontaneous development of molecular tilt $\theta$ with respect to the layer normal decreases the layer thickness. The relation between $d_A$ and $d_C$ is as below,

$$d_C = d_A \cos \delta_C$$

Where $\delta_C$ is the layer tilted angle in SmC* phase.

This contraction of the layers coupled with the no-slip anchoring at the cell boundaries causes a kink to form in the originally uniform layers, producing the chevron structure.

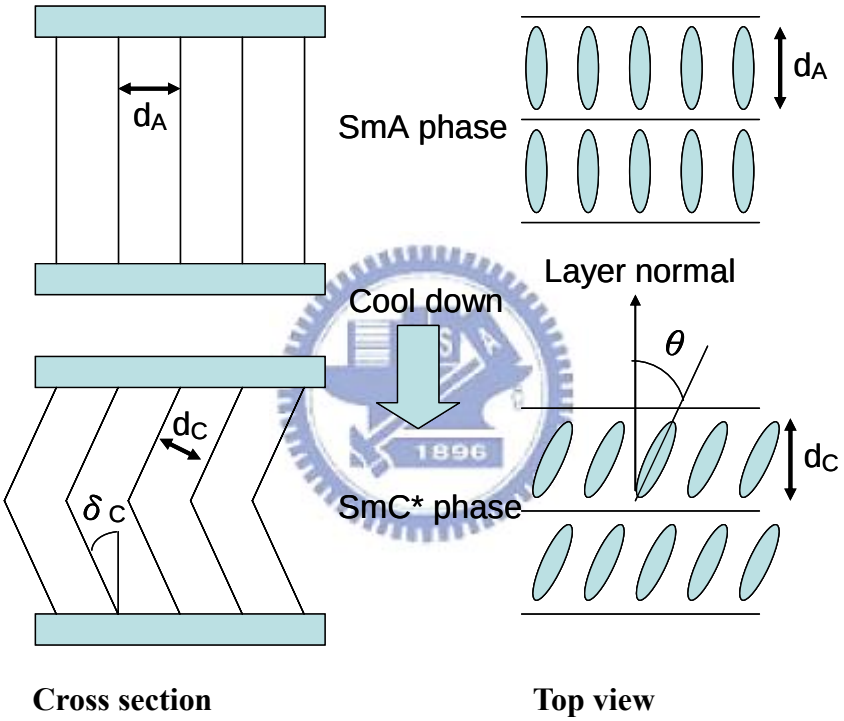


**Fig.2.4.** Origin of the chevron layer structure

Two basic classifications of molecular orientation are based on the relationship between the tilting direction of chevron layer structure and the surface pretilt. The C1 and C2 state are defined by this classification. The C1 and C2 states are easily distinguished by the tilting direction of the chevron layer structure. The tilting direction of chevron is toward rubbing direction is called C2 state. The same reason, if the tilting direction of chevron is opposite to the rubbing direction is called C1 state, as illustrated in Fig.2.5.

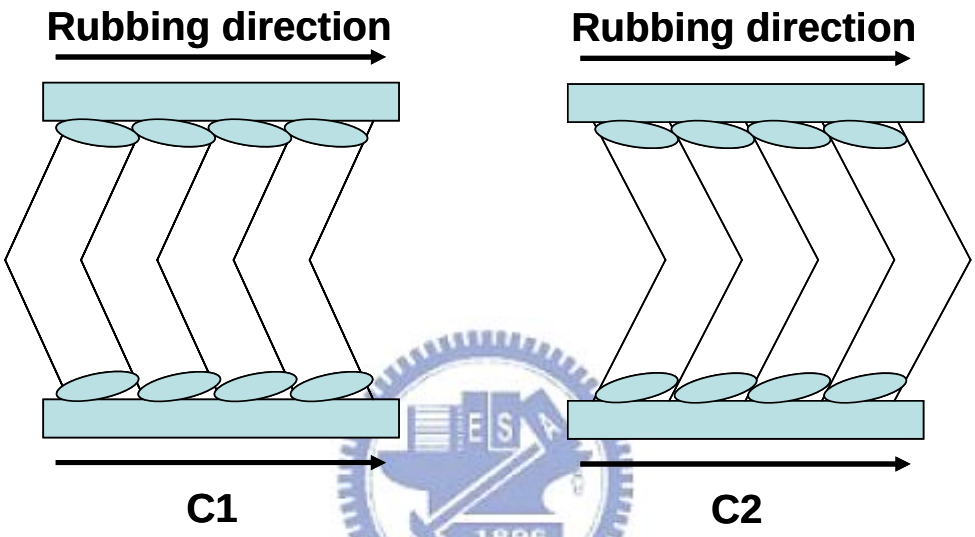


**Fig.2.5.** Two chevron structure: C1 state and C2 state.

Four states [17], C1U (C1-uniform), C1T (C1-twisted), C2U (C2-uniform), and C2T (C2-twisted), were found in SSFLCs treated by parallel rubbing alignment. And one special case of the C2U state is called the high pretilt C2U which shows only one state with extinction position with high pretilt angle aligning films in C2 state, as shown in Fig 2.6. Among all states, the C1U and C2U states are interesting in the practical concept owing to giving the possibility of achieving a better alignment.

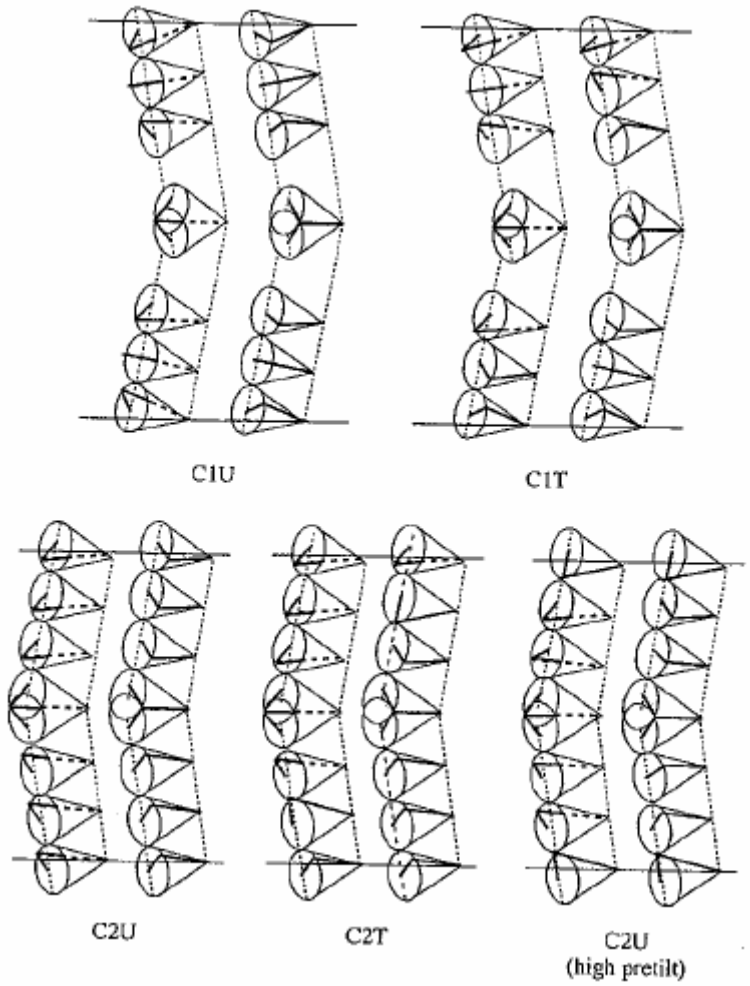


**Fig.2.6.** Molecular orientation modes of the four states are in SSFLC [12].

### 2.2.3 Zigzag Defect

Zigzag formation [12] occurs when domains with chevrons pointing in opposite directions are interspersed as shown in Fig.2.7 (b), because the extinction positions for C1 and C2 are different. The two boundary plates are equally treated and the rubbing directions of the two plates are parallel. C1 is the structure where the chevron apex points opposite to the rubbing direction; C2 is the structure where the chevron apex points toward the rubbing direction. Zigzag shows a hairpin defect and lightning defect as illustrated in the bottom of Fig.2.7 (a). A hairpin defect is produced in the position where the apexes of C1 and C2 adjoin. Lightning defect are generated in the apex of C1 distant from the apex of C2. A hairpin defect usually grows along the smectic layer, and lightning defect are parallel to the rubbing

direction. Zigzag defects seriously degrade the quality of the electro-optical properties of the display.

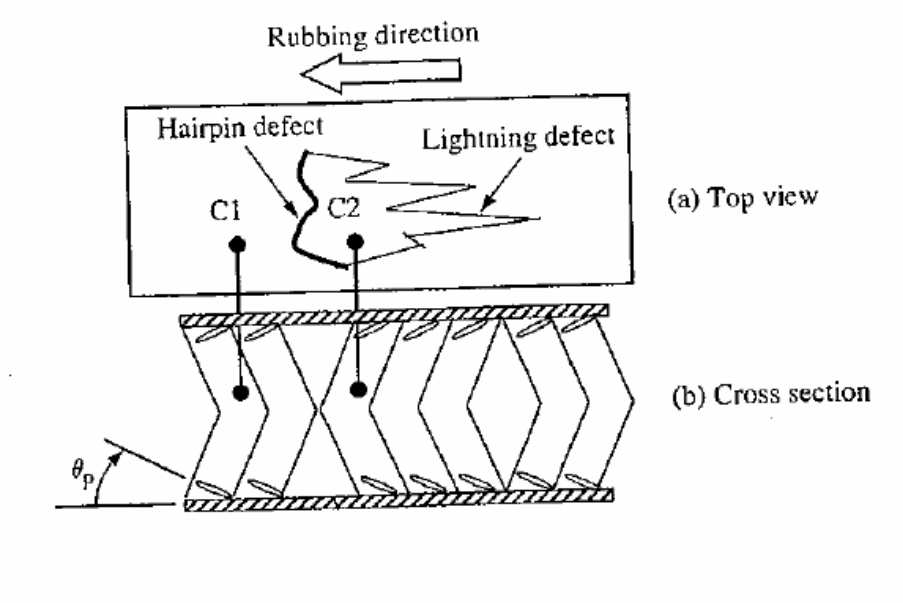


**Fig.2.7.** (a) Top view shows the shape of zigzag. (b)The cross section shows the chevron structure of C1 and C2 states [12].

### 2.2.4 Horizontal Chevron Defect

The horizontal chevron geometry was first reported by Patel and Goodby [18] with cooling across a N*-SmC* transition under DC field conditions. As a consequence of preserving a constant smectic layer thickness, a folding then takes place not across, but in the plane of the cell. Thus horizontal chevron occurs. These are smectic layer structures with the liquid crystal molecules oriented parallel to the rubbing direction, but with the spontaneous polarization in opposite directions in different domains, implying inclined smectic layers with the layer normal oriented at an angle equal to the director tilt angle to either side of the the rubbing direction [19-22]. A schematic representation of this structure is depicted in Fig 2.8.

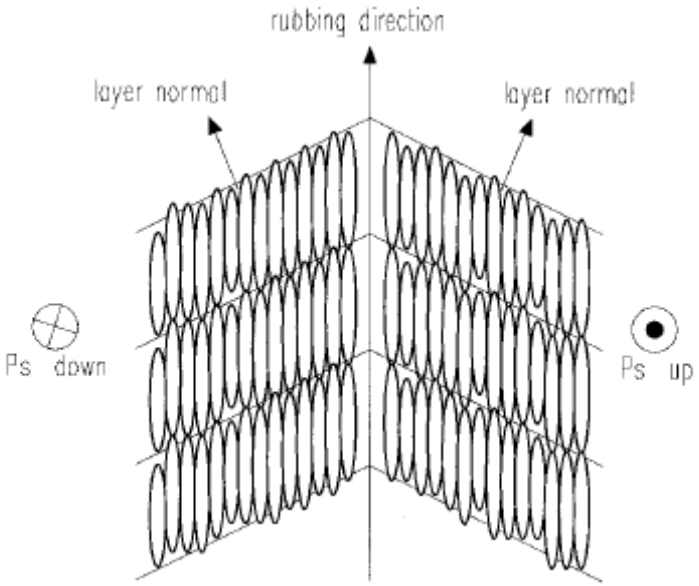


**Fig.2.8.** Schematic illustration of the horizontal chevron domain structure, as a top view in the surface stabilized state with unwound helix [20].

In the multi-domain structure [23], the behavior is clearly presented as shown in Fig 2.9, while applying an electric field. With positive electric field, a certain domain appears dark, while the molecules of the other domain are oriented at an angle $2\theta$ to the rubbing direction and appear bright in Fig 2.9 (a). With no electric field, the molecules of both domains are oriented along the rubbing direction, thus resembling a well oriented bookshelf texture. Regions between the two domains are still visible as defect lines of the chevron in Fig 2.9 (b). Reversal of the electric field as opposed to Fig 2.9 (a), results in the inverse image in Fig 2.9 (c).

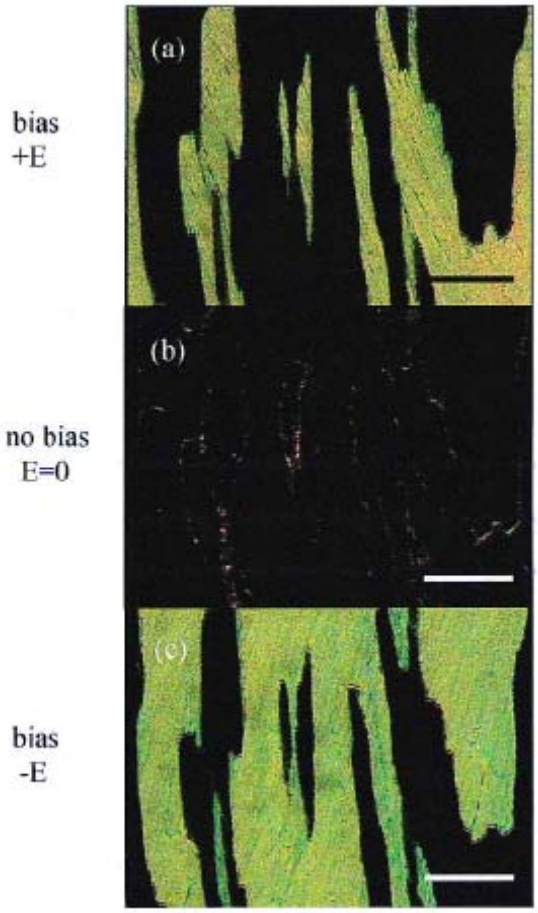


**Fig.2.9.** Horizontal chevron domain structure for (a) applied positive electric field, (b) zero electric field and (c) negative electric field. The bar is equal to 200 $\mu$m [23].

## 2.3 Study of Mono-domain

### 2.3.1 Stable in Uniform State

The stable director orientation of the SSFLC devices in layer-normal geometry by minimizing the total free energy of the surfaces and the bulk elastic distortion with three non-equal elastic constants as functions of cell gap, helical pitch, elastic constant, cone angle and surface interaction coefficient [24-25]. Following the distortion energy density can be written in Oseen-Frank form [26] as

$$W_d = (K_1/2)(\nabla \bullet \hat{n})^2 + (K_2/2)[\hat{n} \bullet (\nabla \times \hat{n}) - q_t]^2 + (K_3/2)[\hat{n} \times (\nabla \times \hat{n}) - q_t]^2 \ldots\ldots\ldots(1)$$

The $K_1, K_2, K_3$ are the splay, twist, and bend elastic constants. Using the cone angle, $2\theta$, the azimuthal angle of the $\hat{c}$ director, $\varphi$, the pitch, P, spontaneous twist, $q_t$, and

spontaneous bend, $q_b$, are given by

$$q_t = -q_o \sin^2 \theta \quad \text{.....(2)}$$

$$q_b = q_o \cos\theta(\hat{n} \times \hat{z}) \quad \text{.....(3)}$$

Where $|q_o| = 2\pi /$ p, and the sign of $q_o$ specifies the handedness of the LC helicoids. The $\hat{n}$ director is expressed as

$$\hat{n} = (\sin\theta\cos\phi, \sin\theta\sin\phi, \cos\theta) \quad \text{.....(4)}$$

Suppose variation of $\phi$ is restricted to the y direction and under the condition of constant cone angle, the operation is following below:

$$\therefore \nabla \bullet \hat{n} = \phi_y \sin\theta\cos\phi \qquad \because (\nabla \bullet \hat{n})^2 = \phi_y^2 \sin^2\theta\cos^2\phi \quad \text{.....(5)}$$

And

$$\nabla \times \hat{n} = \phi_y \sin\theta\sin\phi \ \hat{k},$$

$$\hat{n} \bullet \nabla \times \hat{n} = \phi_y \sin\theta\sin\phi\cos\theta,$$

$$\therefore \hat{n} \bullet \nabla \times \hat{n} - q_t = \sin\theta(\phi_y \sin\phi\cos\theta + q_o \sin\theta)$$

$$\because (\hat{n} \bullet \nabla \times \hat{n} - q_t)^2 = \sin^2\theta(\phi_y^2 \sin^2\phi\cos^2\theta + 2\phi_y q_o \sin\phi\cos\theta\sin\theta + q_o^2 \sin^2\theta) \quad \text{.....(6)}$$

And

$$\hat{n} \times \nabla \times \hat{n} = \phi_y \sin^2\theta\sin^2\phi \ \hat{i} \ - \ \phi_y \sin^2\theta\sin\phi\cos\phi \ \hat{j},$$

$$\therefore \hat{n} \times z = \sin\theta\sin\phi \ \hat{i} \ - \ \sin\theta\cos\phi \ \hat{j}$$

$$\because q_b = q_o \sin\theta\cos\theta\sin\phi \ \hat{i} \ - \ q_o \sin\theta\cos\theta\cos\phi \ \hat{j},$$

$$\therefore \hat{n} \times \nabla \times \hat{n} - q_b = \sin\theta\sin\phi(\phi_y \sin\theta\sin\phi - q_o \cos\theta) \ \hat{i}$$

$$- \ \sin\theta\cos\phi(\phi_y \sin\theta\sin\phi - q_o \cos\theta) \ \hat{j}$$

$$\because (\hat{n} \times \nabla \times \hat{n} - q_b)^2 = \phi_y^2 \sin^4\theta\sin^2\phi - 2\phi_y q_o \sin^3\theta\sin\phi\cos\theta + q_o^2 \sin^2\theta\cos^2\theta \quad \text{.....(7)}$$

Substituting Eq. (5), (6), (7) into Eq. (1) to get the distortion energy density as below:

$$W_d = (\frac{\phi_y^2}{2})\sin^2\theta[K_1\cos^2\phi + (K_2\cos^2\theta + K_3\sin^2\theta)\sin^2\phi]$$
$$+\phi_y q_o(K_2 - K_3)\sin^3\theta\cos\theta\sin\phi \quad \text{……..……(8)}$$
$$+(\frac{q_o^2}{2})\sin^2\theta(K_2\sin^2\theta + K_3\cos^2\theta)$$

Where $\phi_y$ denote the partial derivative of $\phi$ with respect to y. The surface energy per unit area arising from the molecular interactions with the bounding surfaces is given by

$$F_s = \sum_i [r_1^{(i)}(\hat{n}\bullet\hat{s}) + r_2^{(i)}(\hat{p}\bullet\hat{s})] \text{……...(9)}$$

Where $\hat{p}$ and $\hat{s}$ are the unit vectors of the spontaneous polarization and the surface normal. The summation sums from both top and bottom surfaces (i = t, b), $r_1^{(i)}$ and $r_2^{(i)}$ are the non-polar and polar surface-interaction coefficients. Keeping the lowest order terms, it can be expressed as

$$F_s = \sin^2\theta\ (r_1^{(t)}\sin^2\phi_t + r_1^{(b)}\sin^2\phi_b) - r_2^{(t)}\cos\phi_t + r_2^{(b)}\cos\phi_b \text{……....(10)}$$

Where $\phi_t$ and $\phi_b$ are azimuthal angles at the upper and lower surface (y = d / 2 and y = -d / 2).

The total free energy per unit area is thus given by

$$F = \int_{-d/2}^{d/2} W_d\,dy + F_s \text{……....(11)}$$

To minimize the total free energy to obtain the surface-stabilized states, we solve the Euler-Lagrange equation, suppose the simplest solution is $\phi_y = 0$ or $\phi = const.$, which represents the uniform up ($\phi_t = \phi_b = 0$) and down ($\phi_t = \phi_b = \pi$) state.

The total free energy per unit area for the uniform state is given by

$$F_u = \frac{dq_0^2}{2}\sin^2\theta(K_2\sin^2\theta + K_3\cos^2\theta) \mp (r_2^{(t)} - r_2^{(b)}) \text{……...…(12)}$$

Where the – and + signs correspond to up and down states, respectively.

The other solution ($\phi_y \neq 0$), which gives the splay state, the total free energy per unit

area of the splay state can be expressed by

$$F_{spl} = \frac{d}{2} C \sin^2\theta + \frac{dq_o^2}{2} \sin^2\theta (K_2 \sin^2\theta + K_3 \cos^2\theta)$$

$$- q_o (K_2 - K_3) \sin^3\theta \cos\theta (\cos\phi_t - \cos\phi_b)$$
$$+ \sin^2\theta (r_1^{(t)} \sin^2\phi_t + r_1^{(b)} \sin^2\phi_b)$$

$$- r_2^{(t)} \cos\phi_t + r_2^{(b)} \cos\phi_b \quad \text{.....(13)}$$

Another solution ( $\phi = q_o z$ ) is the helical state in a thick cell, the total free energy per unit area of the helical state is given by

$$F_{hel} = \frac{1}{2} (r_1^{(t)} - r_1^{(b)}) \sin^2\theta \quad \text{.....(14)}$$

Then to simulate results, the matter discussion focuses on cell thickness, pitch length, and surface interaction coefficients. From the results, the left handedness helicoid FLC can obtain much better effect of uniform state. As shown in Fig 2.10 (a) is the cell thickness dependent on pitch, it shows that the uniform state prefer to stabilize in thin cell gap at intermediate pitch. With the relation between the cell thickness and surface interaction coefficients as shown in Fig 2.10 (b), the large non-polar coefficient or small polar coefficient can increase the critical cell thickness that the SSFLC cell can stabilize in uniform state.

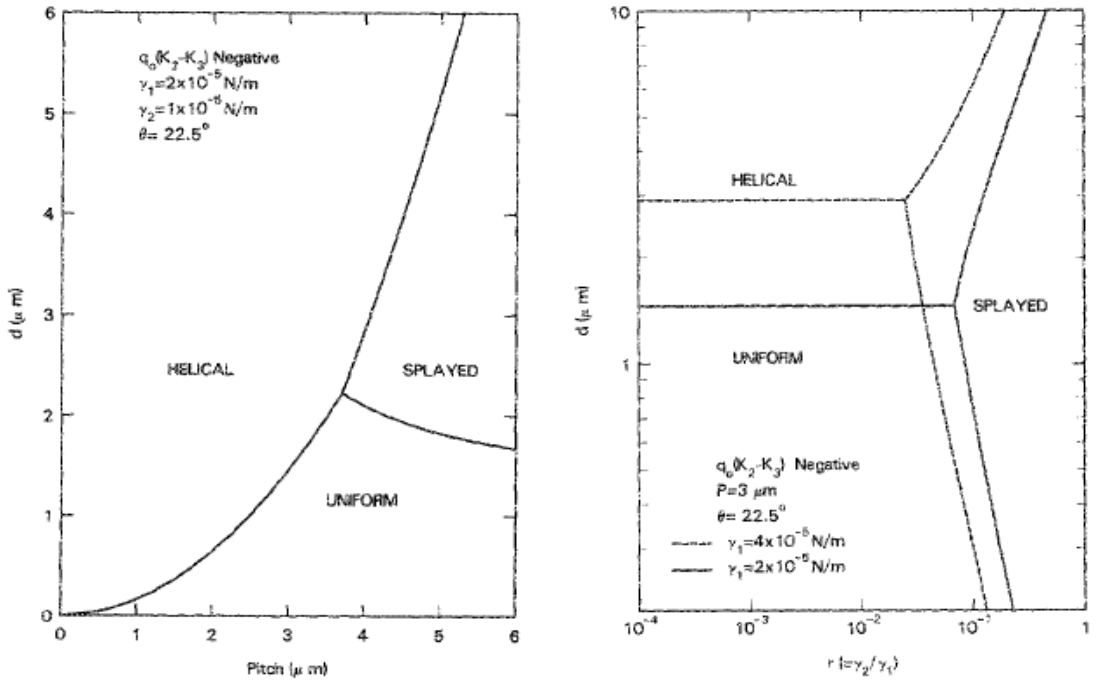


**Fig.2.10.** Phase diagram as a function of (a) cell thickness and pitch, (b) cell thickness and ratio of polar to non-polar coefficients for the left handedness helicoids [24].

### 2.3.2 Zigzag Free Defect

#### 2.3.2.1 C1 uniform orientation

The C1U state as shown in Fig 2.11, it is possible to achieve a zigzag free C1 structure that is also of practical value for using in FLC displays. The C1 orientation was first reported by Kanbe et al. [27] and the C1U orientation was first reported by Koden et al. [28]. They reported that a combination of the high pretilt aligning film and a low tilt angle for the FLC material is required to obtain the C1U state and prevent the appearance of the C2 state. On the other hand, Hanyu et al. have reported that the cross-rubbing technique is useful for producing a uniform C1U state by avoiding the appearance of C1T [29]. In the application of display, Koden et al. [30] and Tsuboyama et al. [31] showed good display performance with a uniform C1U orientation by using a high pretilt alignment layer with a low tilt FLC material.

### 2.3.2.2 C2 uniform orientation

The C2 orientation was first reported by Kanbe et al. [27] and the C2U orientation (shown in Fig 2.11) was first reported by Koden et al. [28]. Two useful approaches to realizing the formation of a C2U orientation have been reported. One approach involves an investigation of the method of alignment. The C2 orientation is possible in the low pretilt angle condition, but it's impossible in the high pretilt angle condition. Strong rubbing has also been reported as being favorable to producing the C2 orientation [32-33] because the direction of molecules on a surface in the C2 orientation become almost the same as the direction of rubbing and that is insensitive to variations in alignment, surface polarity, memory effects, and surface switching. The other approach is to investigate the relationship between the properties of materials and the formation of C2 orientation. To obtain the C2 orientation, a material must be in the SmA phase over a wide range of temperatures. This is because the FLC materials are in SmA phase over a wide range of temperature tend to have small tilt angles near the SmC to SmA transition point. This small tilt angle can reduce the energy barrier for transition from the C1 to the C2 state near the SmC to SmA transition point because the small tilt angle leads to chevron layers leaning at a small angle. On the other hand, Furue et al. adopted polymer-stabilized method to obtain defect free C2U orientation [34].

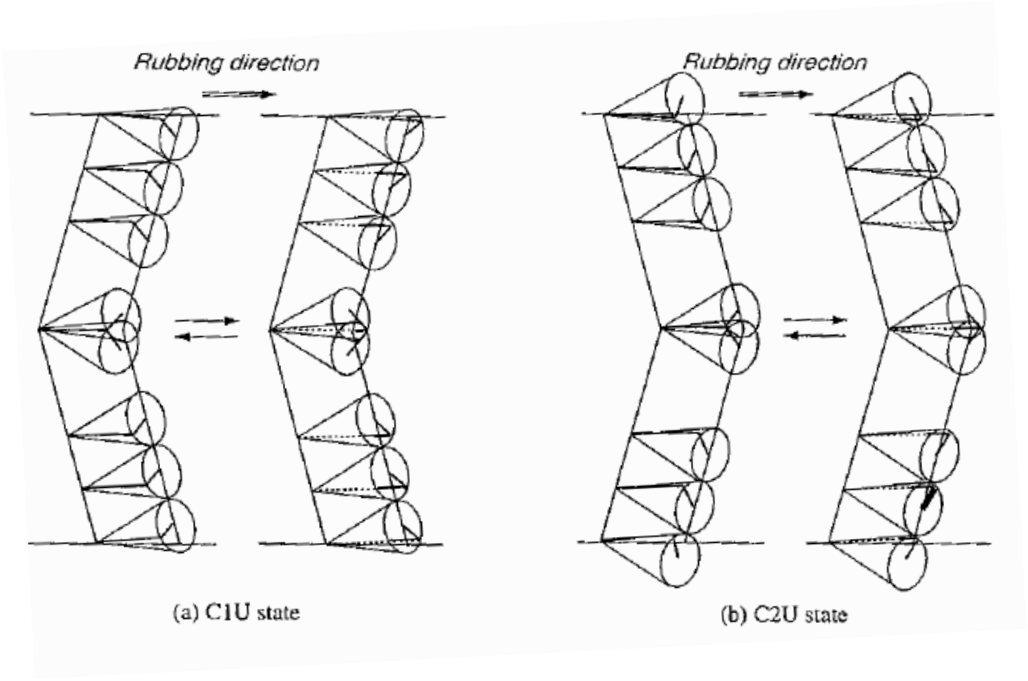


**Fig.2.11.**

Molecular orientation in C1U and C2U state [12].

### 2.3.2.3 Bookshelf orientation

The bookshelf layer structure as shown in Fig 2.12, is the ideal molecular orientation for SSFLC. One of the greatest merits of the bookshelf layer structure is its wide memory angle. The wide memory angles are suitable for display applications that require high contrast ratio and high brightness. Three major approaches have been investigated to obtain a bookshelf layer structure.

First approach is AC-field treatment [35]. An initial chevron layer structure is turned into a bookshelf layer structure by applying a strong low frequency AC field. High Ps of FLC material is required because the interaction between the electric field and Ps induces a torque that changes the layer structure from chevron to bookshelf.

Second approach is to utilization a unique class of materials with tilt angles that are weakly dependent on temperature. In the previous section, the chevron layer structure is the reduction of layer spacing brought about by cooling. The reduction of layer spacing is usually observed in FLC materials with an INAC (Iso – N – A – C) phase sequence; because the tilt

angles of such FLC materials are usually strongly dependent on temperature. However, there is a unique of FLC materials in which the tilt angle is not strongly dependent on temperature. Mochizuki et al. reported that certain FLC mixtures that include an FLC compound with a naphthalene ring will take on a quasi-bookshelf layer structure [36]. They reported that the temperature range over which material was in the SmA phase was increased and that zigzag defects tended to disappear as the concentration of the naphthalene compound was increased.

Third approach utilizes FLC materials with an INC (Iso – N – C) phase sequence, and the DC voltage applied during the material cools and changes from the N to SmC phase [37-38]. The quasi-bookshelf orientation is suitable for active matrix drive method, because it exhibits mono-stable and a smooth V-T characteristic. This mode is called CDR (continuous director rotation) or Half-V shaped FLC [35-39].

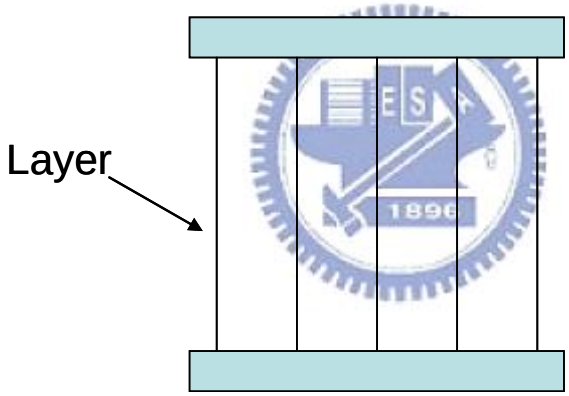


**Fig.2.12.** Bookshelf layer structure.

### 2.3.3 Eliminate Horizontal defect

The polarity of the alignment layer surface has much influence on alignment phenomena for FLC materials, the sign of the polarity is defined as negative when the dipole on the surface is directed toward from the surface to the liquid crystalline material for the positive FLC materials as shown in Fig 2.13 [40]. The sign of the polarity on the alignment layer can be determined by using the dissymmetric cell with the two different alignment layers by Dijon [41], the other method of determining the alignment layer polarity by Takatoh et al [42].

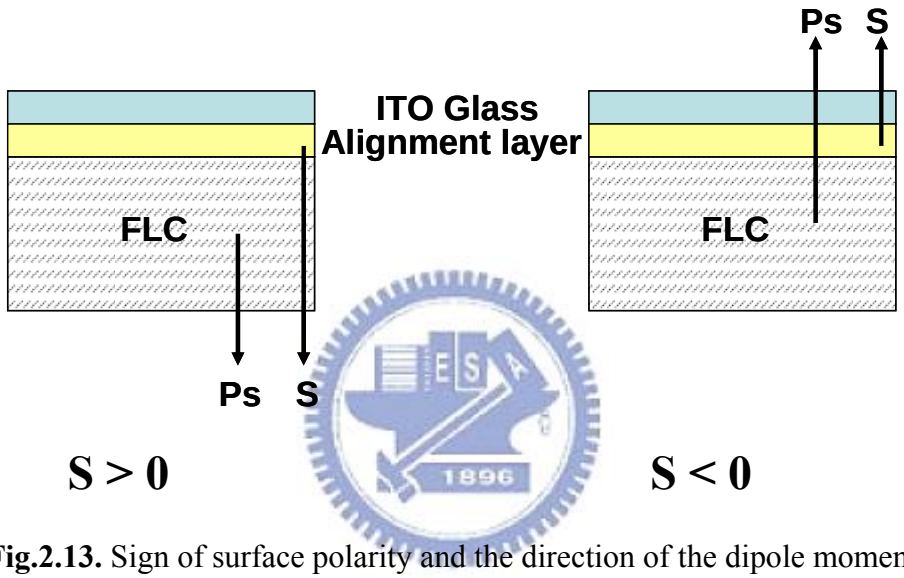


**Fig.2.13.** Sign of surface polarity and the direction of the dipole moment.

The horizontal chevron defect with two different layers usually occurs in a symmetric structure cell with the same alignment layer and rubbing strength on both ITO glass. In order to solve this problem, an asymmetric cell with two different polarity of alignment layer (PVA and PI) is used in our study. This cell structure is called as hybrid cell, and the hybrid cell is expected to generate the below model as shown in Fig 2.14. Because the PI can induce the upper direction of Ps to direct outward of the surface and vice versa in bottom plate, one smectic layer maybe formed in the parallel rubbing.

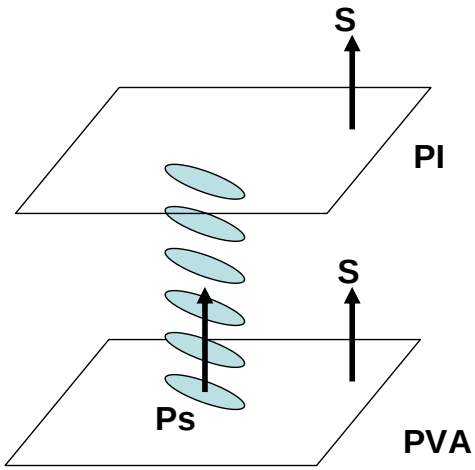


**Fig.2.14.** Hybrid cell with combination the positive (PVA) and negative (PI) alignment layers.

## 2.4 Summary

Molecular orientation is a very important factor in determining the performance of a display in the development of practical FLC displays. In previous description realizes the molecule orientation state and the causes of zigzag and horizontal defect. Next, we discuss how to eliminate defects and stabilize in uniform state related to the SSFLC device. Finally, the proposed methods are effective to improve the alignment ability in our research.

# Chapter 3

# Fabrication process, Instruments

## 3.1 Introduction

This chapter will describe fabrication process and instruments in study. The fabrication is divided into two parts, one part of mix material; one part of make Hybrid cell. The instruments have UV/Vis Spectrometer (PerKin Elmer), Laser System, AFM (Veeco), POM, DSC (PerKin Elmer), LCAS-1 (LC vision), the function and operation method of measurement tools will describe in following sections, and tools were characterized the properties of the filled SSFLC cell.

## 3.2 Fabrication process

Two fabrication processes include to mix materials and to make Hybrid cell. To prepare R3206 and R3206H, R3206 mixtures were made by mixing R3206H, the R3206H has the same phase sequential temperature as R3206 without chirality. On the made Hybrid cell, 2.5%wt. PVA and 50%wt. were prepared in fabrication process, the PVA and PI have different polarity as alignment layer. The detail steps of two fabrication processes will describe in following sections.

### 3.2.1 R3206 mixtures Preparation

Step1: On the electronic scale, the desirable weight of R3206 and R3206H were put together in a 20ml vial.

Step2: The mixture were dissolved by using glass rod to stir it on the hotplate at 120 ℃.

### 3.2.2 Hybrid cell fabrication

The major of processes is presented as shown in Fig. 3.1.

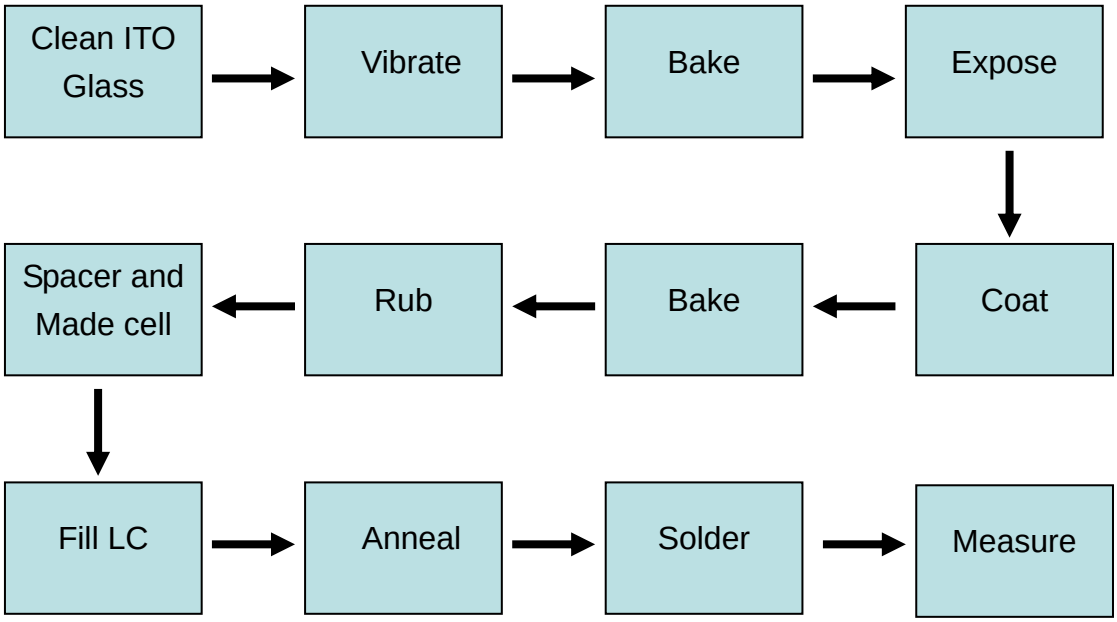


Fig. 3.1. Cell fabrication processes of sketch diagram

Step1: The ITO glass was washed by using detergent.

Step2: The ITO glass was vibrated for 30 minutes by using supersonic oscillator.

Step3: On the ITO glass, the water of surface was blow off with nitrogen gas firearm, then put it on hotplate and bake it for 30 minutes at 110 ℃.

Step4: The UV-ozone treated surface of ITO glass for 20 minutes that is for better adhesion of alignment layer.

Step5: Put the ITO glass on the spin coater. To drop the solvent of alignment material (Chisso Company NB-32 for polyimide, di-water for PVA) onto the whole area of ITO glass, next wait 30 seconds, then spin. After spin-coating, to drop the solution of alignment material (Chisso Company PIA-X660-01X, Aldrich company PVA) onto the whole area of ITO glass, next wait 30 seconds, then spin. The spin rate is as follows:

| 2.5wt.%PVA | | | Polyimide | | |
|---|---|---|---|---|---|
| | Rate | Time | | Rate | Time |
| 1st | 500rpm | 30s | 1st | 500rpm | 30s |
| 2nd | 1500rpm | 60s | 2nd | 5000rpm | 60s |

Step6: To put the ITO glass on the hotplate and bake it for 1 hour at 200 ℃.

Step7: To rub the ITO glass with rubbing machine, the parameter of rubbing strength is used as below:

| 2.5wt.%PVA | | Polyimide | |
|---|---|---|---|
| Pile impression | 0.23mm | Pile impression | 0.2mm |
| Rotation rate | 300rpm | Rotation rate | 300rpm |
| Advancing rate | 7.3mm/s | Advancing rate | 7.3mm/s |

Step8: To prepare 1.6 $\mu$m of spacer, the small amount of spacer dropped six dots at the edge of bottom glass. Then, cover the top glass and press. Next, place the cell under a UV lamp for 5 minutes to fully cure, and to measure a cell gap by using spectrometer UV-Vis 650 (from Perkin Elmer).

Step9: Heat up the FLC material until the temperature exceeded the clearing point. Inject the FLC material into the empty cell until the FLC is full of the gap.

Step10: To anneal the FLC cell with programmable hotplate, the annealing process depends on the phase sequence of the LC material. The parameter of annealing is used as below:

| Material | Iso temp. (waiting time) | N* temp. (waiting time) | SmC* temp. (waiting time) |
|---|---|---|---|
| R3206 | 120℃ (5min) | 95℃ (5min) | 65℃ (30min) |
| 70%R3206 | 120℃ (5min) | 95℃ (5min) | 65℃ (30min) |
| 50%R3206 | 120℃ (5min) | 95℃ (5min) | 65℃ (30min) |
| 20%R3206 | 120℃ (5min) | 95℃ (5min) | 65℃ (30min) |
| 10%R3206 | 120℃ (5min) | 95℃ (5min) | 65℃ (30min) |

Step11: To solder the wire at the top and bottom ITO by using ultrasonic soldering device (KURODA TECHNO Co.,Ltd).

Step12: Then the characteristic of FLC cell was measured by using measurement instruments.

## 3.3 Measurement Instruments

In this chapter, the brief introductions of instruments and principle will be described in this section. The surface morphology was examined by AFM. The gap of empty cell was measured by spectrometer UV-Vis 650. The alignment texture of R3206 mixtures were observed by POM. The spontaneous polarization was characterized by LCAS-1. The mesophase temperature of R3206 mixtures were measured by DSC, and the E-O properties and contrast ratio were characterized by laser system.

### 3.3.1 UV/Vis Spectrometer

The UV-VIS Spectroscopy is as shown in Fig 3.2, LAMBDA 650 PerKin Elmer is high performance between 190 nm and 900 nm with the resolution $\leqq$ 0.17 nm, and the spectrometer principles are double-beam, double monochromator, ratio recording spectrophotometers.

Fig. 3.2. Instrument of UV-VIS Spectroscopy, LAMBDA 650 PerKin Elmer.

The absorption, reflectance and transmittance of materials characterized with LAMBDA 650, and the large sample compartment allows easy access to a wide variety of sampling accessories.

The principle of interference method [43] is used to measure cell gap. The concept of the measurement method is based on the interference pattern of the light reflected by a layer with two reflecting surfaces. Assume the situation as described in Fig.3.3. The coefficient of reflection R1 is defined as the ratio of the light reflected by surface 1 to the total incident light on surface 1. Surface 2 has a coefficient of reflection R2.

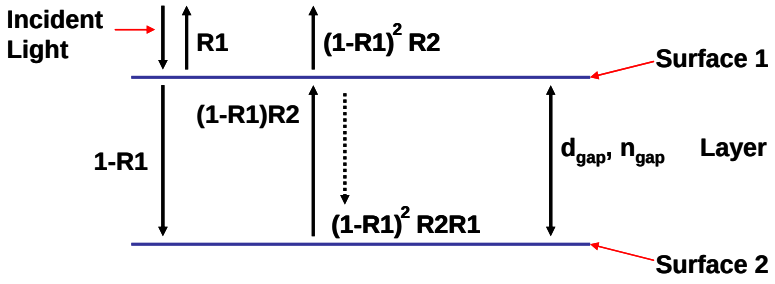


Fig. 3.3. Two reflecting surfaces separated by a layer causing a light interference. The dotted line indicates the first internal reflection.

The incident light is $I = \cos \omega t$ and to assume there is no absorption of light in surface 1 and surface 2, so we can get the total reflected light R is

$$R = R_1 \cos \omega t + \sum_{k=1}^{\infty} R_1^{k-1} R_2^{k} \left(1 - R_1\right)^{1+k} \cos \omega \left(t - k t_o\right) \quad \text{..... (3-1)}$$

$$\omega = 2\pi c n_{gap}^{\frac{1}{2}} / \lambda$$

$$t_0 = 2 d_{gap} n_{gap}^{\frac{1}{2}} / c$$

Where c, $\lambda$, $d_{gap}$ and $n_{gap}$ are the speed of light in the vacuum, the wavelength, the cell thickness and the refractive index. The cosine factor are caused by internal reflections in Eq. (3-1) for k>1. Since R1<1 and R2<1, the magnitude of the cosine factors for k>1 is much smaller than for k=1. Consequently, the internal reflections is neglected and the total reflected light R can be expressed as

$$R = R_1 \cos \omega t + \left(1 - R_1\right)^2 R_2 \cos\left(\omega t - \frac{4\pi n_{gap} d_{gap}}{\lambda}\right) \quad \text{.....(3-2)}$$

The reflected spectrum is

$$\left|R(\lambda)\right|^2 = R_1^{\,2} + \left[\left(1 - R_1\right)^2 R_2\right]^2 + 2R_1\left(1 - R_1\right)^2 R_2 \times \cos\left(4\pi n_{gap} d_{gap} / \lambda\right) \quad \text{.....(3-3)}$$

The periodic term in Eq.(3-3) causes what is generally known as an interference pattern. The periodicity of the reflected interference spectrum clearly determines the optical thickness of the cell gap, $n_{gap} d_{gap}$.

If the $\lambda_1$ and $\lambda_2$ are the two wavelengths yielding extrema in Eq.(3-3), then $\cos\left(4\pi n_{gap} d_{gap} / \lambda\right) = \pm 1$ for $\lambda = \lambda_1$ and $\lambda = \lambda_2$. And

$$2 n_{gap} d_{gap} = k_1 \lambda_1 / 2 \quad \text{.....(3-4)}$$

$$2 n_{gap} d_{gap} = k_2 \lambda_2 / 2 \quad \text{.....(3-5)}$$

Where $k_1$ and $k_2$ are natural numbers. Suppose $\lambda_1 > \lambda_2$, then

$$k_2 = k_1 + x \quad \text{.....(3-6)}$$

Where x is a natural number.

Based on Eqs.(3-4), (3-5), and (3-6), we can write

$$n_{gap}d_{gap} = \frac{x\lambda_1\lambda_2}{4(\lambda_1 - \lambda_2)} \quad \text{.....(3-7)}$$

Between the wavelengths $\lambda_1$ and $\lambda_2$, the value of x-1 indicates the number of extrema in $|R(\lambda)|^2$. In theory $n_{gap}d_{gap}$ can be determined if the wavelengths for a consecutive maximum and minimum (x=1) are known. If several wavelengths with extrema are known, to choose the distance x is better between the two extrema as large as possible. These results improve the accuracy of the calculation of $n_{gap}d_{gap}$ in a bigger difference $\lambda_1$- $\lambda_2$ in the denominator of Eq. (3-7).

As the interference data of Fig. 3.4, in the air ($n_{gap} = 1$), to choose the peaks of 693 nm and 476 nm, and the numbers of peak between them and themselves are 5, thus the gap of this cell is:

$$1 \bullet d_{gap} = \frac{(5-1) \bullet 693 \bullet 476}{4(693-476)} \Rightarrow d_{gap} = 1.52 \ \mu\text{m}$$

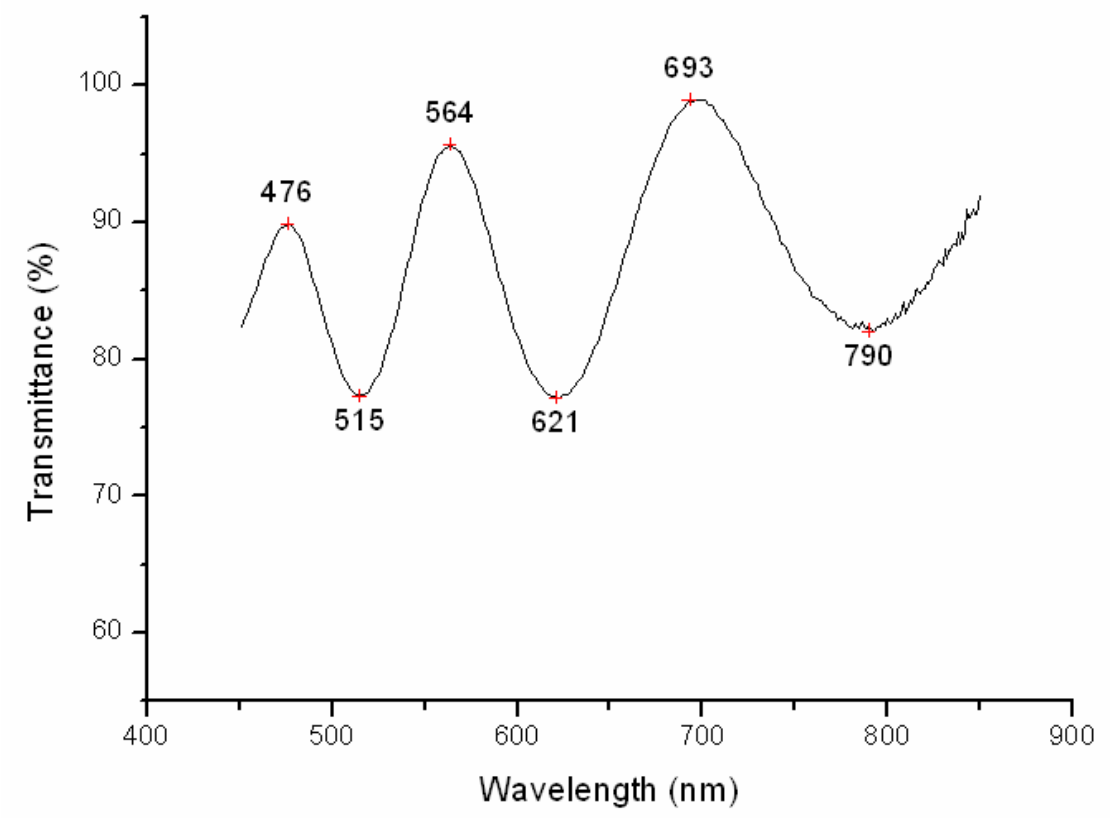


Fig. 3.4. Interference data of one Hybrid cell by UV-Visible

### 3.3.2 Laser system

The laser system is as shown in Fig.3.5. This laser system can measure Volt-Transmittance characteristics, response time, stable state and contrast ratio. He-Ne laser ($\lambda = 632.8$nm) is the light source, and the intensity of laser has to reduce within the acceptable range of the photo detector by using a 10% ND filter. Test cell is placed on rotation stage between the cross-polarizer, and driven by waveform generator, WFG500 (FLC ELECTRONICS AB) which is operated with computer. A hot-stage (METTILER TOLEDO) can provide the desired temperature with an accuracy of ±0.10℃. The various electro-optic properties are performed with the photo-detector (FLC ELECTRONICS AB), and the results are exhibited with oscilloscope.

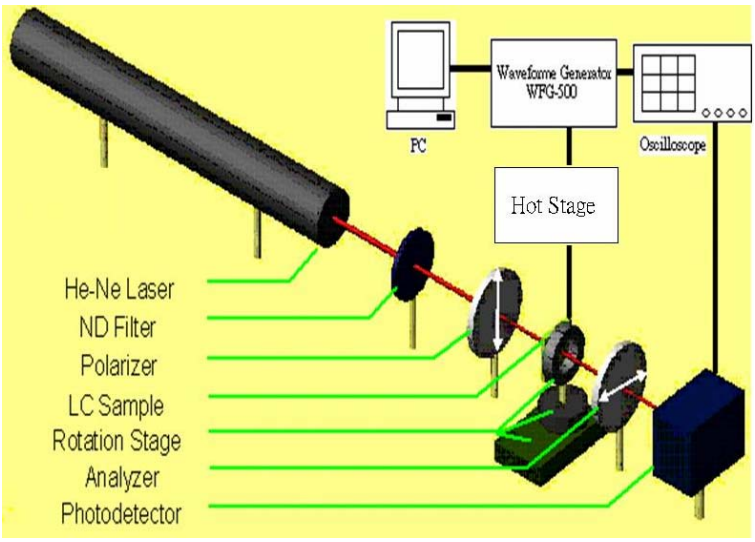


Fig. 3.5. Diagram of laser system.

### 3.3.3 POM

The POM, OLYMPUS BX51 is as shown in Fig 3.6. Alignment textures were observed under POM with the magnifications of 100X, and the transparent mode is utilized with bottom light source. Next, the images were captured in the computer by CCD. Others application, distance and area can be calculated with its software.

Fig. 3.6. Instrument photo of POM.

### 3.3.4 AFM

The AFM has a number of advantages that it provides easily achievable high-resolution and three-dimensional information in real space with little sample preparation for low-cost. In-situ observations, imaging in fluids, temperature and environmental controls are all available.

Illustrated in the Fig 3.7 [44], AFM works by bringing a cantilever tip in contact with the surface to be imaged. An ionic repulsive force from the surface applied to the tip bends the cantilever upwards. The amount of bending is measured by a laser spot reflected on to a split photo detector, can be used to calculate the force. By keeping the force constant while scanning the tip across the surface, the vertical movement of the tip follows the surface profile and is recorded as the surface topography by the AFM. There are three primary modes of AFM:

First mode is contact mode AFM that operates by scanning a tip attached to the end of a cantilever across the sample surface while monitoring the change in cantilever with a split photodiode detector. The tip contacts the surface through the adsorbed fluid layer on the sample surface. A feedback loop maintains a constant deflection between the cantilever and the sample by vertically moving the scanner at each (x,y) data point to maintain a “setpoint” deflection. By maintaining a constant cantilever deflection, the force between the tip and the sample remains constant. The force is calculated from Hooke’s Law: F = -kx where F = force, k = spring constant and x = cantilever deflection. Force constants usually range from 0.01 to 1.0 N/m, resulting in forces ranging from nN to uN in an ambient atmosphere. The distance the scanner moves vertically at each (x,y) data point is stored by the computer to form the topographic image of the sample surface. Operation can take place in ambient and liquid environments.

Second mode is tapping mode AFM that operate by scanning a tip attached to the end of an oscillating cantilever across the sample surface. The cantilever is oscillated at or near its resonance frequency with amplitude ranging typically from 20nm to 100nm. The frequency of oscillation can be at or on either side of the resonant frequency. The tip lightly "taps" on the sample surface during scanning, contacting the surface at the bottom of its swing. The feedback loop maintains constant oscillation amplitude by maintaining a constant RMS of the oscillation signal acquired by the split photodiode detector. The vertical position of the scanner at each (x,y) data point in order to maintain a constant "setpoint" amplitude is stored by the computer to form the topographic image of the sample surface. By maintaining constant oscillation amplitude, a constant tip-sample interaction is maintained during imaging. Operation can take place in ambient and liquid environments. In liquid, the oscillation need not be at cantilever resonance. When imaging in air, the typical amplitude of the oscillation allows the tip to contact the surface through the adsorbed fluid layer without getting stuck.

Third mode is non-contact mode AFM, the cantilever is oscillated at a frequency which is slightly above the cantilever's resonance frequency typically with an amplitude of a few nanometers (<10nm), in order to obtain an AC signal from the cantilever. The tip does not contact the sample surface, but oscillates above the adsorbed fluid layer on the surface during scanning. The cantilever's resonant frequency is decreased by the van der waals forces, which extend from 1nm to 10nm above the adsorbed fluid layer, and by other long range forces which extend above the surface. The decrease in resonant frequency causes the amplitude of oscillation to decrease. The feedback loop maintains a constant oscillation amplitude or frequency by vertically moving the scanner at each (x,y) data point until a "setpoint" amplitude or frequency is reached. The distance the scanner moves vertically at each (x,y) data point is stored by the computer to form the topographic image of the sample surface.

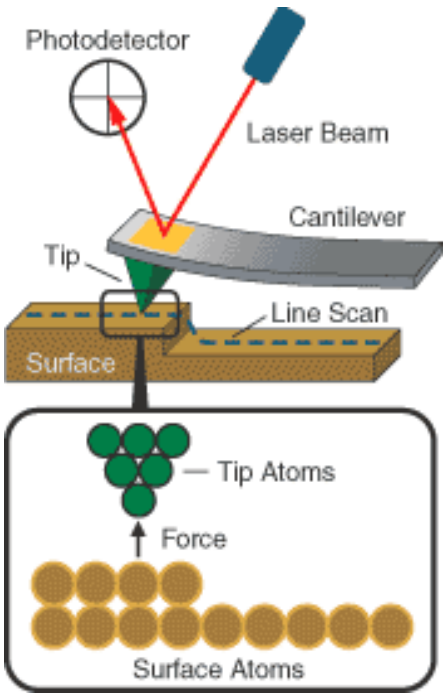


Fig. 3.7. Illustration of AFM principle [44].

### 3.3.5 DSC

The Pyris Diamond DSC [45] is as shown in Fig 3.8, and its functionality is following:

a. Unique power-compensation design

b. Highest caloric accuracy

c. Superior signal resolution and sensitivity

d. Multiple cooling options for a temperature range of -170 ˚C to 725 ˚C

e. 44 position Auto sampler for unattended operation

f. HyperDSC™, the leading fast scan DSC technique

g. StepScan, for Modulated Temperature DSC

The DSC was utilized to characterize the thermal properties of material with the power-compensation principle. With power-compensation DSC, the sample and the reference material are placed in separate, self-contained calorimeters. When the temperature rises or falls in the sample material, power (energy) is applied to or removed from the calorimeter to compensate for the sample energy. As a result, the system is maintained at a "thermal null" state at all times.

The amount of power required to maintain system equilibrium is directly proportional to the energy changes occurring in the sample. No complex heat-flux equations are necessary with a power-compensation DSC because the system directly measures energy flow to and from the sample. 3-10mg R3206 mixtures were put in the aluminum pan, and it was analyzed at heating and cooling rate 10℃/min. Phase transition temperatures were defined with the endothermic peaks in the heating curve and exothermic peaks in the cooling curve.

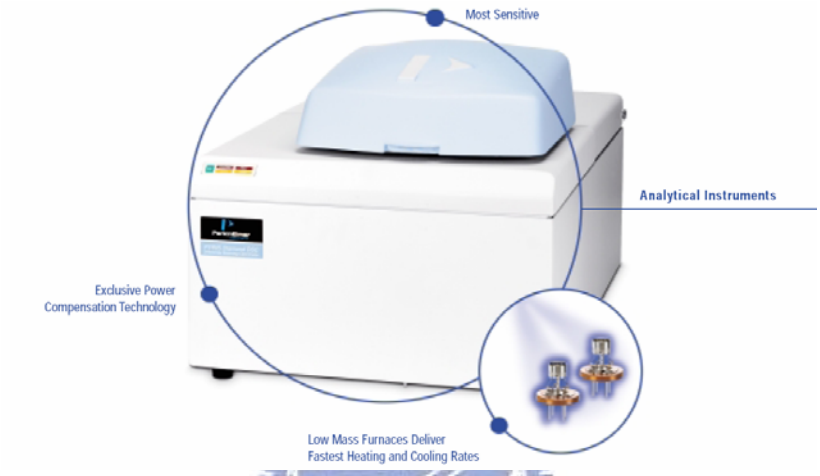


Fig. 3.8. Instrument photo of DSC.

### 3.3.6 LCAS-1

The value of spontaneous polarization was characterized by using LCAS-1 under 5 $\mu$m pre-made cells (from LC Vision). The theory of LCAS-1 uses the current nulling method to measure the resistance and capacitance of the test cell. The equivalent circuit of the measurement circuit is shown in Fig. 3.9. The simplified model of the test cell is a parallel RC circuit. The applied voltage produces a current through the resistive and capacitive cell elements. This current would normally go into the input of the current amplifier as the sum of the resistive and capacitive currents. However, the LCAS-1 contains an adjustable resistive and capacitive element connected from the input of the amplifier to a voltage source that is of equal amplitude and opposite polarity of the voltage applied to the test cell. The resistive and capacitive components are adjusted until the current through these elements is equal to the

current through the test cell components. When this condition is achieved, the current into the current amplifier is zero or null. Thus this condition is referred to as a current null.

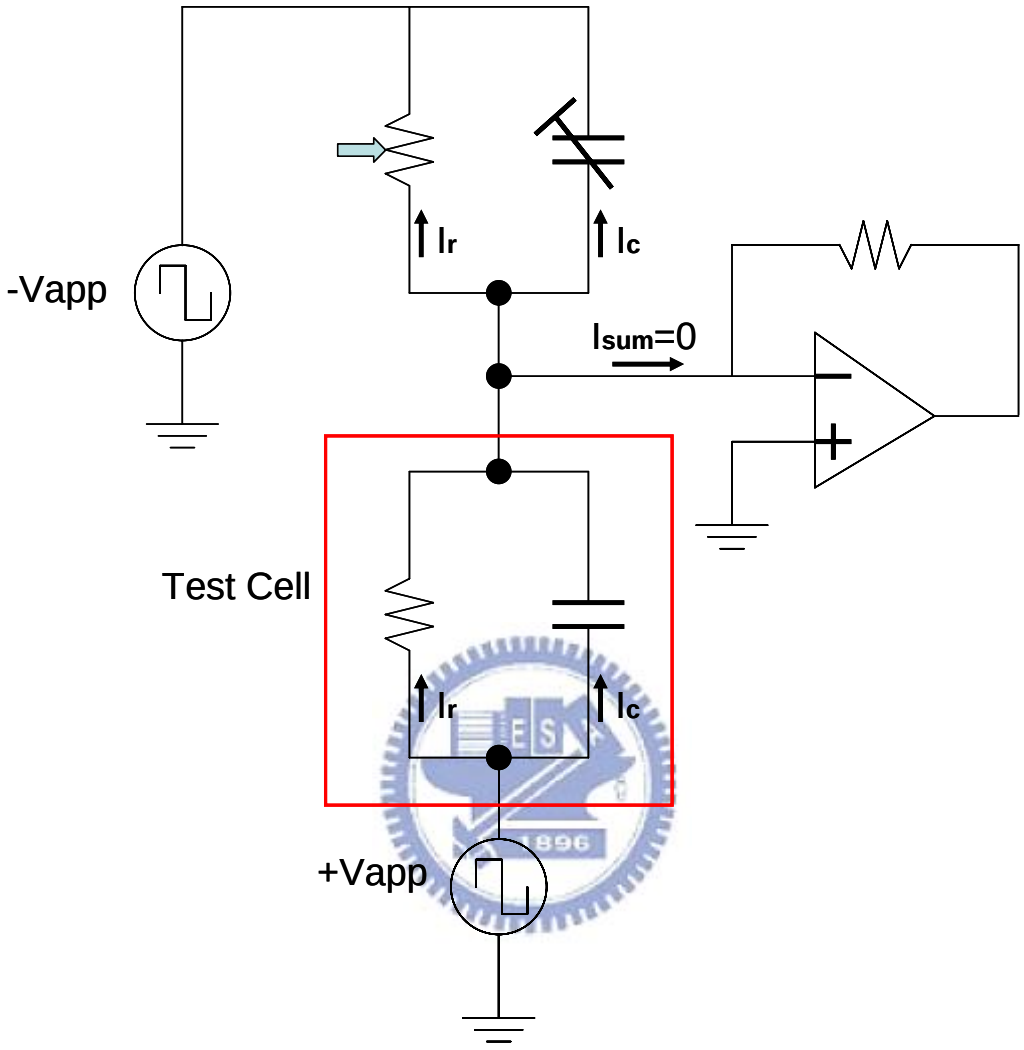


Fig. 3.9. Illustration of LCAS-1 principle.

# Chapter 4

# Experimental Results and Discussion

## 4.1 Introduction

The R3206 was utilized with the advantage of low driving voltage (Vsat = 3.5V), different weight percentage R3206 mixtures were investigated. We discuss the experimental results of R3206 mixtures, the thermal properties were characterized with differential scanning calorimetry (DSC). Electro-optical properties and the alignment textures were characterized under 2 $\mu$m pre-made cell (from EHC) and hybrid cell with laser system and polarizing optical microscope (POM), respectively. The surface properties were measured by atomic force microscope (AFM), and the spontaneous polarization was characterized with liquid crystal analysis system (LCAS-1) under 5 $\mu$m pre-made cell (from LC vision).

## 4.2 Thermal properties

Thermal properties of ferroelectric liquid crystal (R3206), smectic C host (R3206H) and mixtures were measured by using DSC at cooling rate 10 $^{o}$C /min, the mesophase temperature of R3206, R3206H and their mixtures were listed in Table 1. The mesophase of nematic and smectic C were presented in R3206H, and the R3206 possesses cholesteric and chiral smectic C phase. The R3206 and R3206H have wide SmC* (SmC) temperature from 79.45 $^{o}$C to -17.90 $^{o}$C and 73.77 $^{o}$C to -29.73 $^{o}$C, respectively. To mix two kinds of material, the thermal properties of 70 wt.% (R3206_70) and 50 wt.% (R3206_50) possess the mesophase temperature range of R3206 and R3206H without optically active components.

Table 4.1. Phase sequence temperature of pure compounds and mixtures were obtained from DSC at cooling rate at 10 °C /min.

| Materials | Phase sequence temperature ( ˚C ) |
|---|---|
| R3206H | Iso 110.66 ─ N 73.77 ─ SmC -29.73 Cry |
| R3206 | Iso 109.88 ─ N* 79.45 ─ SmC* -17.90 Cry |
| R3206_70 | Iso 109.39 ─ N* 76.81 ─ SmC* -21.85 Cry |
| R3206_50 | Iso 110.63 ─ N* 77.19 ─ SmC* -23.39 Cry |

**Iso : Isotropic, N : Nematic, Sm : smectic, Cry : Crystalline, * : chiral**

## 4.3 Surface morphology

The results were shown in Fig 4.1 and Fig 4.2 by using Atomic Force Microscope. Topographic images were obtained by scanning an area of $20 \times 20\ \mu m^2$ for both samples. The mean roughness (Ra) of 50%wt. polyimide calculated with 1.086 nm, and the thickness of 50wt. polyimide had 25 nm. However, the mean roughness of PVA was smoother than 50%wt. polyimide with 0.908 nm, and the thickness of PVA had 95 nm.

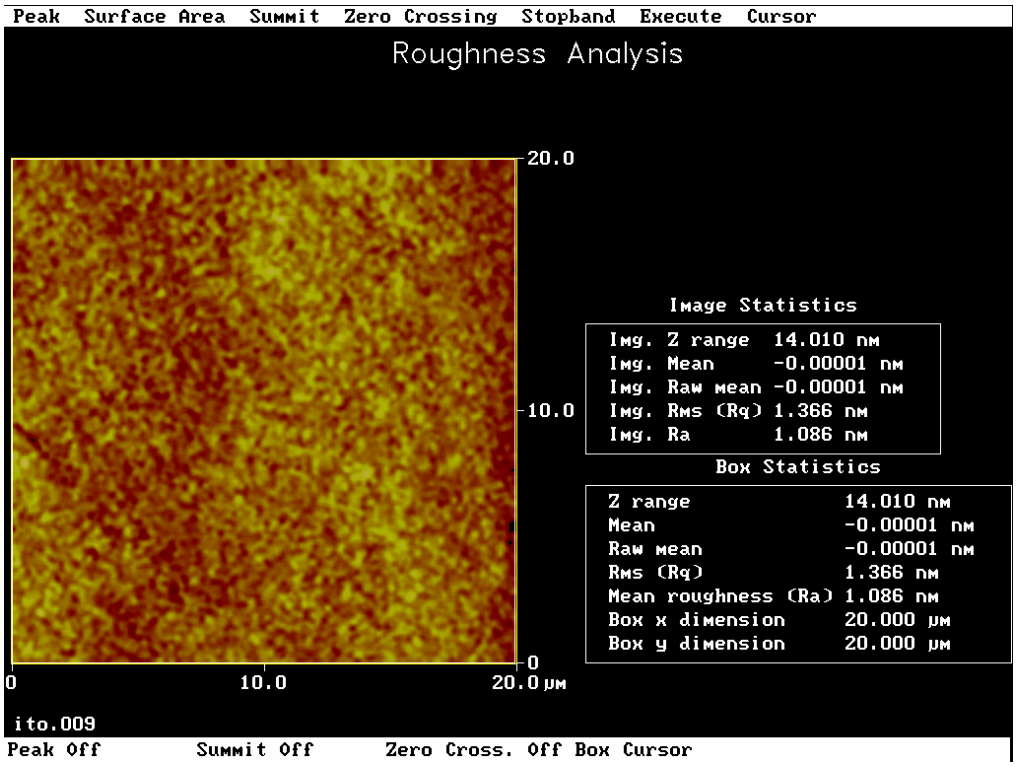


Fig. 4.1. Surface morphology of 50 weight percentage polyimide.

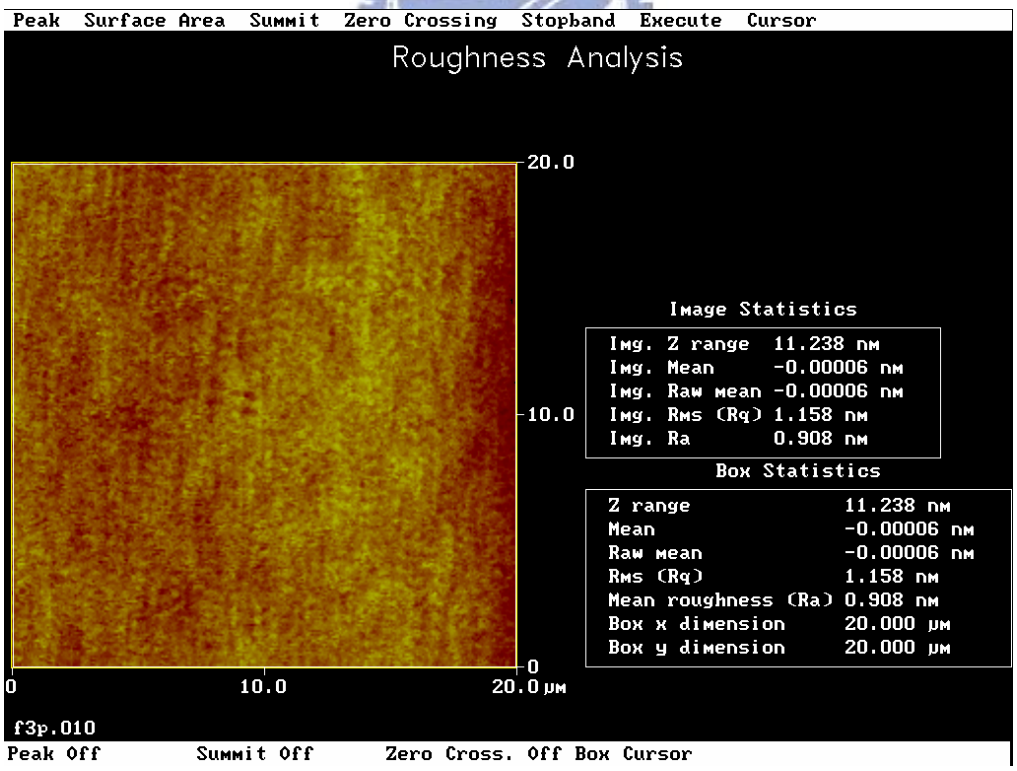


Fig. 4.2. Surface morphology of 2.5 weight percentage PVA.

## 4.4 Alignment ability

In elastic-continuum energy theory [25-27], the FLC structures have uniform, helix, and splay state. Besides, only uniform and helix state exist in the thin cell gap. From the pitch and cell gap relation, the free energy of uniform state is inversely proportional to the square of the pitch length while the free energy of helical state is independent of the pitch length. Therefore, the former will decrease and become smaller than the later with pitch elongation. The FLC molecular arrangement prefers to stay in uniform state, which is more stable at low energy.

In order to improve R3206 alignment, we increased the pitch by diluting R3206 mixtures [11,46]. The polarizing optical microscope (POM) pictures of each sample in the pre-made cells (1.8 $\mu$m, from EHC) were captured and shown in Fig. 2. The pure R3206 showed poly-strip domain all over the sample, indicated in Fig. 4.1(a). On the contrary, diluted R3206 showed larger domain size with fewer horizontal chevron defects, as shown in Fig. 4.1(b), 4.1(c), and 4.1(d). As a result, the alignment issue of R3206 was improved by the method of pitch lengthening. Among these mixtures, the alignment had the best result as the weight percentage of R3206 lower than 70%.

Asymmetrical hybrid alignment technique or asymmetrical cells [46-48] eliminated alignment defects. Instead of liquid crystal polymers (LCPs) and linearly-photo-polymerized polymers (LPPs), poly vinyl alcohol (PVA) and polyimide (PI, from Chisso) were applied in this study. As shown in Fig. 4.2(a), the uni-direction layer structure was formed with micro-domain in R3206 hybrid cell. And the horizontal chevron defects of R3206_70 were eliminated in hybrid cell as shown in Fig. 4.2(b). The alignment of R3206 and R3206_70 were greatly improved by the asymmetrical hybrid alignment cell approach compared to symmetric cell in Fig. 4.1(c).

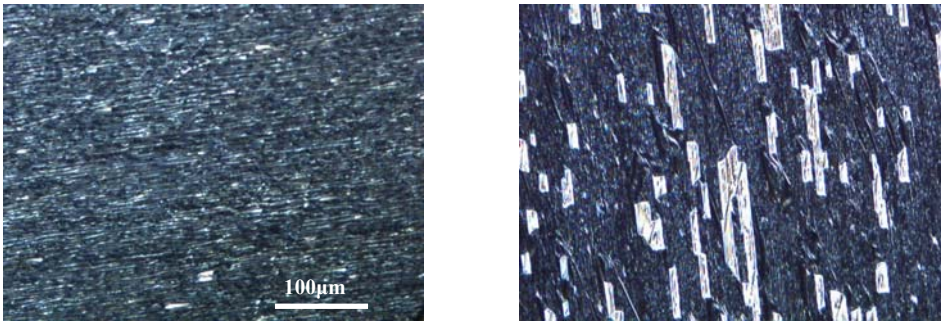


(a) (b)

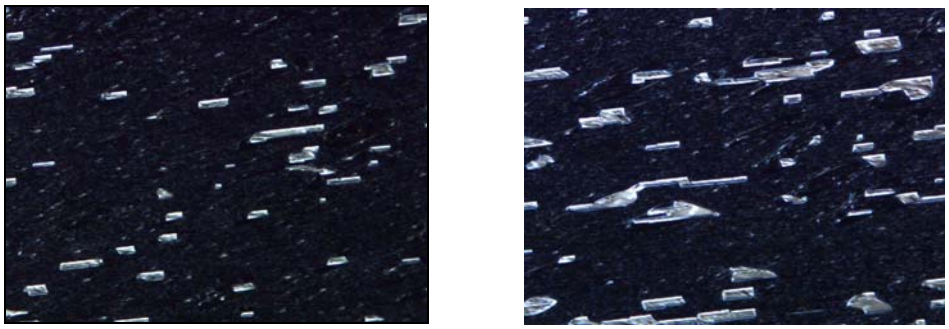

(c) (d)

Fig. 4.3. Microscopic textures of alignment (a) R3206, (b) R3206_80 (c) R3206_70 (d) R3206_50.

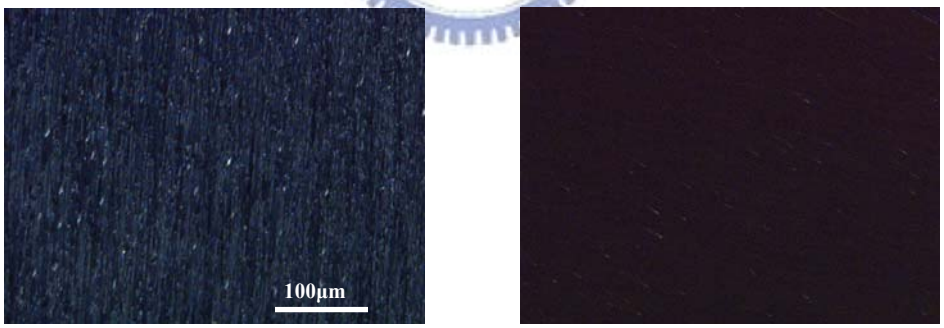


(a) (b)

Fig. 4.4. Microscopic textures of alignment in hybrid cells

## 4.5 Spontaneous polarization and saturation voltage

The spontaneous polarization (Ps) was characterized by applying 30V, 100Hz bipolar square wave under 5 μm pre-made cells (from LC Vision). The peaks were appeared in the result of R3206_70 mixture at 25 ˚C, the Ps values are almost linearly increased with the weight percentage of R3206 as shown in Fig. 4.5.

The saturation voltage (Vsat.) was characterized by driving 8V, 100Hz continuously increase square wave under 1.8 μm pre-made cell (from EHC). Thus, the wave form was applied at R3206_70 mixture as shown Fig. 4.6. The Vsat. is increased with decreased spontaneous polarization [11] as presented in Fig. 4.5. Among these mixtures, the R3206_70 still possesses a characteristic of low driving voltage about 4.4V, and its Ps was $12.73\,nC/cm^2$.

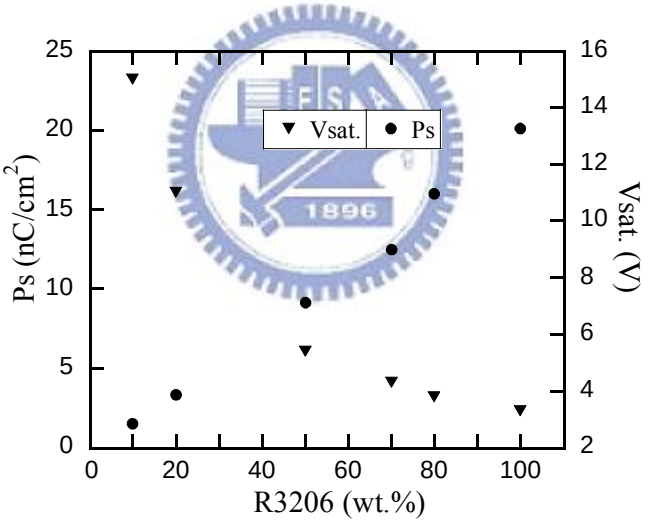


Fig. 4.5. Spontaneous polarization and saturation voltage of R3206 and mixtures.

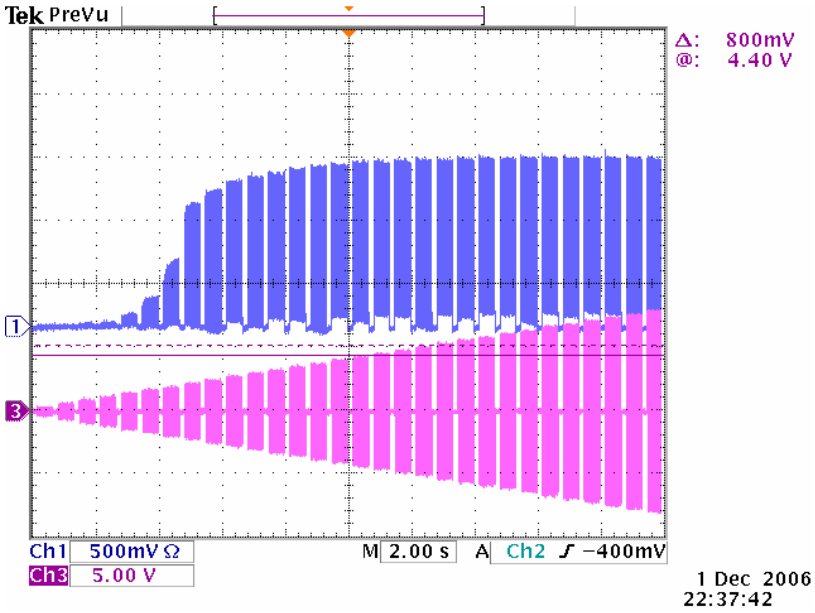


Fig. 4.6. Saturation voltage of R3206_70 driven by 8V, 100Hz continuously increase square wave.

## 4.6 Electro-Optical Properties

Electro-optical properties were characterized by 100Hz square as presented in Fig. 4.7. R3206, R3206_70 and R3206_50 mixture respectively possess threshold voltage over 0.9V, 1.4V and 1.8V, at the same time, the saturation voltages are about 3.5V, 4.3V and 5.8V in the pre-made cell. Lower transmittance in R3206 may be due to the light leakage from poly-strip domain defects. Even thought used hybrid cell, the E-O property of R3206_70 did not have much variation. Triangular driving waveform confirms that both mixtures are half-V switching mode FLC materials as indicated in Fig. 4.8.

Response time ( $\tau$ 10- $\tau$ 90) was characterized with laser system by applying 5V, 100 Hz bipolar square wave as listed in Table 2. Pure R3206 showed a fast response time, the rise time and fall time were 152μs and 520μs, respectively. The R3206_70 and R3206_50 mixture with fast response (response time is about 1.1ms and 1.3ms, respectively) is suitable for color sequential displays among the prepared samples. And the R3206_70 of hybrid cell has the same fast response properties. Pure R3206, R3206_70, R3206_50 and R3206_20 presented

extremely fast response under 155 us, 267 us, 510 us and 1.471 ms respectively when over driven by 14V, 100Hz bipolar square wave as shown in Fig 4.9.

The electro optical characteristics of R3206_70 mixture at different temperature driven by 5V, 100Hz continuously increase square wave as shown in Fig 4.11. Unlike ordinary FLC materials, which have a SmA phase in their phase transition sequence, a half-V FLC material without SmA phase does not show a continuous decrease of the switching angle with temperature [47-48]. The R3206 exhibits that the transmittance is insensitive in variation of temperature.

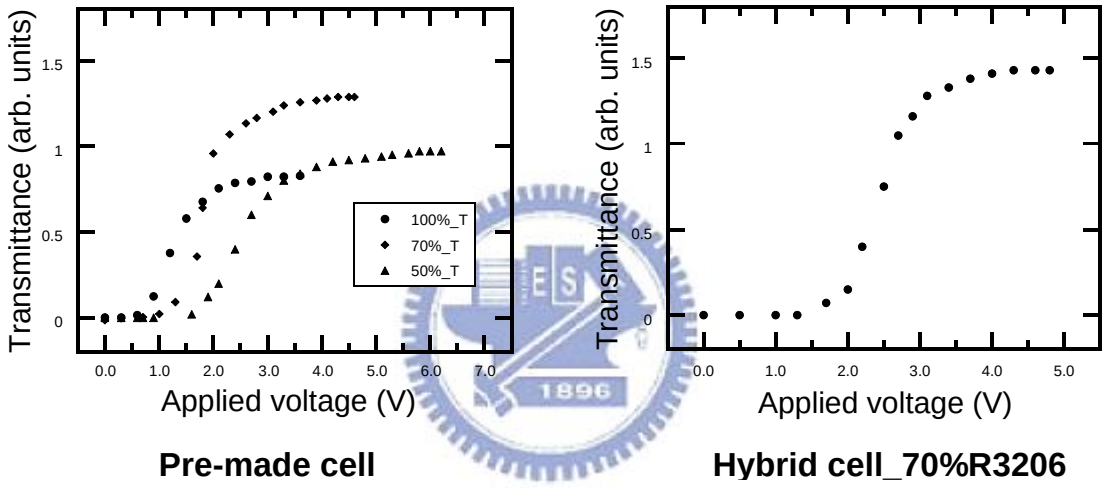


Fig. 4.7. Electro-optic properties of R3206, R3206_70 and R3206_50 driven by 100Hz square wave.

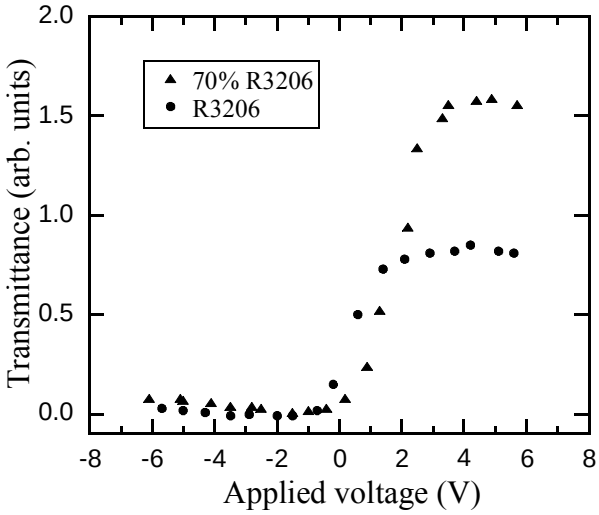


Fig. 4.8. V-T characteristics of an H-V-mode of R3206 and R3206_70 mixtures, driven by 30Hz triangular wave.

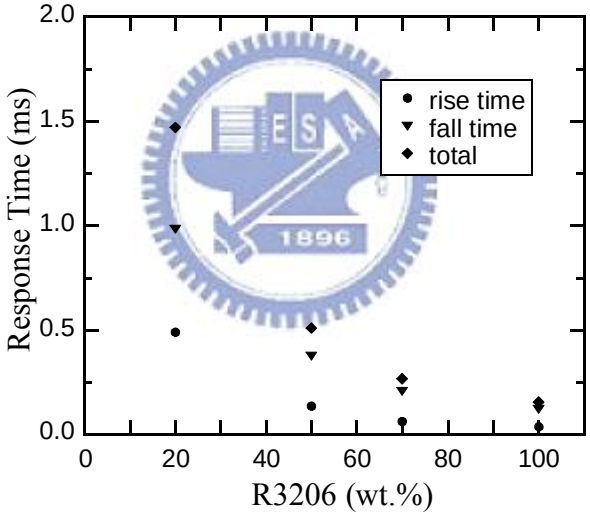


Fig. 4.9. Response time of different wt.% of R3206 mixtures in 1.8±0.1μm pre-made cell, driven by 100 Hz, 14V square wave.

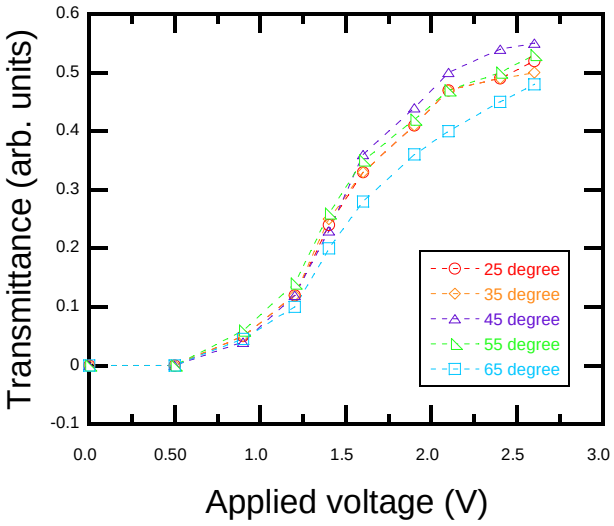


Fig. 4.10. Electro-Optic characteristics of R3206_70 mixture driven by 5V, 100Hz continuously increase square wave at different temperature.

Table 2. Response time of various FLC samples in 1.8μm cell, driven by 100Hz, 5V bipolar square wave.

| Material | Rise time (μs) | Fall time (μs) |
|---|---|---|
| R3206 | 152 | 520 |
| R3206_70 | 240 | 850 |
| R3206_50 | 380 | 920 |

## 4.7 Contrast ratio, Cone angle and Stable state

The contrast ratio (CR) and Stable state were characterized with waveform generator WFG500 (made in FLC ELECTRONICS AB) by using laser system under crossing polarizer. Contrast ratio of R3206_70 was improved from 68 to 263 by hybrid cell. Mono-stable of materials were confirmed by applying special waveform as shown Fig 4.10. The FLC material R3206 exhibits the switching angle of 31 degrees as listed in table 3. If the Cone angle can rise from 31 to 45 degrees, the Contrast ratio would be improved with increase of transmittance.

Table 3. The other characteristic of various FLC samples in 1.8μm cell, driven by 100Hz, 5V bipolar square wave.

| Material | Contrast ratio (a.u.) | Cone angle (˚) | Stable state |
|---|---|---|---|
| R3206 | 57 | 31 | M |
| R3206-70 | 68 | 31 | M |
| R3206-70 (hybrid cell) | 263 | 31 | M |

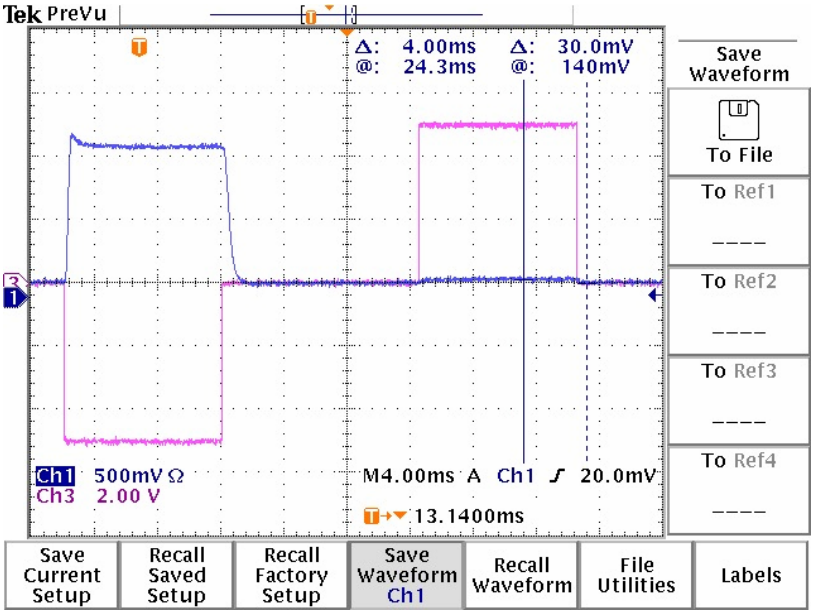


Fig. 4.11. V-T characteristics of a Mono-stable state of R3206_70 hybrid cell, driven by 100Hz, 5V bipolar wave.

## 4.8 Summary

Low driving voltage and clean aligned FLC display is achieved by combining treated FLC material and special surface pre-treatment. The R3206-70 FLC material was suitable for TFT application with the advantage of low driving voltage and fast switching below 5V and 1.1 ms, respectively. The alignment issue of R3206 was improved by pitch lengthening and asymmetrical hybrid cell. The diluted R3206 mixtures possessed relatively good domain and better contrast in SSFLC devices. Furthermore, the horizontal chevron defects could be suppressed by asymmetrical hybrid alignment cell and greatly improved the contrast ratio of R3026-70 from 68 to the best result of 750. Therefore, a desirable low driving voltage, well aligned and fast response FLC material can be applied in the active matrix TFT-FLC display and be able to realize full color sequential display.

# Chapter 5
# Conclusions

## 5.1 Summary

In this thesis, we found approaches to overcome these problems. First, we utilized a Half-V FLC material R3206 with low driving voltage to solve zigzag defect, because the Half-V FLC tilt angle are weakly dependent on temperature that may realize a bookshelf layer structure without electrical field. The pure R3206 showed poor alignment which was poly-strip domain. Base on concept that makes the molecular orientation stabilize in uniform state, so we proposed an improving alignment method that is to increasing pitch lengthening by diluted R3206. The diluted R3206 mixtures showed larger domain size with horizontal chevron defects as the weight percentage of R3206 lower than 70%. Next, the horizontal chevron defect was successful suppressed by using an asymmetry hybrid cell in R3206_70. Our results have many advantages of high contrast ratio, fast switching, low driving voltage, wide viewing angle, wide operating temperature and weakly influence of EO depends on temperature which provide promising SSFLC device for TFT-LCD application.

## 5.2 Future Works

We have successfully overcome alignment issue by applying elastic continuum theory and surface polarity method. In the future, the surface attracts or repulses the Ps is required to be deeply studied. Thereby, the several important parameters of SSFLC device such as polar and non-polar coefficients of alignment layer, anchoring energy and pitch length can help us to understand the interaction of molecular and surface. On the other hand, the FLC materials have large Ps and small Ps whether the Ps affects the alignment or not in the hybrid cell structure.

# Reference


[1] Y. Tanaka, Y. Taniguchi, T. Sasaki, A. Takeda, Y. Koibe, K. Okamoto, *SID Digest*, 2901 (1998)

[2] Y. Tanaka, Y. Taniguchi, T. Sasaki, A. Takeda, Y. Koibe, K. Okamoto, *SID Digest*, 180 (1999)

[3] K. H. Kim, K. Lee, S. B. Park, J. K. Song, S. Kim and J. H. Souk, Asia Display, 383 (1998)

[4] Y. Mishima, T. Nakayama, N. Suzuki, M.Ohta, S. Endoh, Y. Iwakabe and H. Kagawa, SID Digest, 260 (2000).

[5]K. Ono, Y. Imajo, I. Mori, R. Oke, S. Kato, K. Endo and H. Ishino, SID Digest, 1848 (2005)

[6] C. J. Yu, C. Jeong and S. D. Lee, J. Soc. Inf. Display, 14, 537 (2006)

[7] R. Hasegawa, Y. Kidzu, I. Amemiya, S. Uchikoga and H. Wakemoto, SID Digest, 995 (2007)

[8] T. Fujisawa, M. Hayashi, H. Hasebe, K. Takeuchi, H. Takatsu and S. Kobayashi, SID Digest, 663 (2007)

[9] N. Koma, T. Miyashita, T. Uchida and N. Mitani, SID Digest, 632 (2000)

[10] Noel A. Clark and Sven T. Lagerwall, Appl. Phys. Lett., 36, 899 (1980)

[11] L. M. Blinov, V. G. Chigrinov, ”Electrooptic Effects in Liquid Crystal Materials”, Springer-Verlag, New York, 1993

[12] K. Takatoh, M. Hasegawa, M. Koden, N. Itoh, R. Hasegawa and M. Sakamoto, ”Alignment technologies and applications of liquid crystal devices”, Taylor and Francis (2005)

[13] Y. Ouchi, J. Lee, H. Takezoe, A. Fukuda, K. Kondo, T. Kitamura and A. Mukoh, Jpn. J. Appl. Phys, 27, 1993 (1988)

[14] Y. Ouchi, J. Lee, H. Takezoe, A. Fukuda, K. Kondo, T. Kitamura and A. Mukoh, Jpn. J. Appl. Phys, 27, 725 (1988)

[15] T. P. Rieker, N. A. Clark, G. S. Smith, D. S. Parmar, E. B. Sirota and C. R. Safinya, Phys Rev. Lett., 59, 2658 (1987)

[16] N. Vaupotic, S. Kralj, M. Copic and T. J. Sluckin, Phys Rev. E, 54, 3783 (1996)

[17] M. Koden, H. Katsuse, A. Tagawa, K. Tamai, N. Itoh, S. Miyoshi and T. Wada, Jpn. J. Appl. Phys, 31, 3632 (1992)

[18] J. S. Patel and J. W. Goodby, J. Appl. Phys., 59, 2355 (1986)

[19] I. Dierking, J. Phys., 12, 2657 (2000)

[20] I. Dierking, L. Komitov, S. T. Lagerwall, T. Wittig and R. Zentel, Liq. Cryst., 26, 1511 (1999)

[21] J. S. Patel, S. D. Lee and J. W. Goodby, Phys Rev. A, 40, 2854 (1989)

[22] I. Dierking, F. Giebelmann, J. Schacht and P. Zugenmaier, Liq. Cryst., 19, 179 (1995)

[23] I. Dierking, L. Komitov and S. T. Lagerwall, Liq. Cryst., 24, 769 (1998)

[24] T. C. Chieu, J. Appl. Phys., 64, 6234 (1988)

[25] T. Tsuchiya, H. Takezoe and A. Fukuda, Jpn. J. Appl. Phys, 25, 27 (1986)

[26] C. W. Oseen, Trans. Faraday Soc., 29, 883 (1933)

[27] J. Kanbe, H. Inoue, A. Mizutome, Y. Hanyuu, K. Katagiri and S. Yoshihara, Ferroelectrics, 114, 3 (1991)

[28] M. Koden, T. Shinomiya, N. Itoh, T. Kuratate, T. Taniguchi, K. Awane and T. Wada, Jpn. J. Appl. Phys, 30, 1823 (1991)

[29] Y. Hanyu, K. Nakamura, Y. Hotta, S. Yoshihara and J. Kanbe, SID Digest, 364 (1993)

[30] M. Koden, T. Numao, N. Itoh, M. Shiomi, S. Miyoshi and T. Wada, Proc. Japan Display, 579 (1992)

[31] A. Tsuboyama, Y. Hanyuu, S. Yoshihara and J. Kanbe, Proc. Japan Display, 53 (1992)

[32] M. Koden, T. Furukawa, M. Kabe, S. Okamoto, A. Sakaigawa, T. Sako, M. Sugino, A. Tagawa, J. C. Jones, M. H. Anderson, P. E. Dunn, J. R. Hughes, K. P. Lymer, V. Minter, K. G. Russel and A. J. Slaney, SID Digest, 778 (1998)

[33] J. Xu, R. Kurihara and S. Kobayashi, Jpn. J. Appl. Phys, 40, 4626 (2001)

[34] H. Furue, Y. Iimura, H. Hassebe, H. Takatsu and S. Kobayashi, Proc. IDW, 209 (1998)

[35] A. Hotta, R. Hasegawa and K. Takatoh, Jpn. J. Appl. Phys, 43, 6243 (2004)

[36] A. Mochizuki, K. Motoyoshi and M. Nakatsuka, Ferroelectrics, 122, 37 (1991)

[37] Y. Asao, T. Togano, M. Terada, T. Moriyama, S. Nakamura and J. Iba, Jpn. J. Appl. Phys, 38, 5977 (1999)

[38] T. Nokaka, J. Li, A. Ogawa, Liq. Cryst., 26, 1599 (1999)

[39] T. Furukawa, M. Shigeta, H. Uchida and M. Koden, Proc. IDW, 251 (2000)

[40] B. O. Myrvold, Ferroelectrics, 85, 25 (1988)

[41] J. Dijon, C. Ebel and L. Mulatier, Ferroelectrics, 85, 47 (1988)

[42] K. Takatoh, H. Nagata and T. Saishu, Ferroelectrics, 179, 173 (1996)

[43] F. Bruyneel, H. D. Smet, J. Vanfleteren and A. V. Calster, Opt. Eng., 40, 259 (2001)

[44] Molecular Imaging: http://www.molec.com/what_is_afm.html

[45] Perkin Elmer Precisely: http://www.perkinelmer.ca/fr-CA/default.htm

[46] S. S. Bawa, A. M. Biradar and S. Chandra, J. Phys. D: Appl. Phys., 20, 476 (1987).

[46] M. Okabe, N. Sawatari, M. Ishikawa, H. Hama, SID Digest, 1084 (2005)

[47] S. Kobayashi, J. Xu, H. Furuta, Y. Murakami, SID Digest, 1272 (2003)

[48] Y. Murakami, H. Furuta, J. Xu, H. Endoh, H. Fukuro and S. Kobayashi, Jpn. J. Appl. Phys., 42, 2759 (2003)